A Classification Of Mediterranean Cyclones Based on Global Analyses

Oreste Reale [1]
Goddard Earth Sciences and Technology Center,
University of Maryland Baltimore County
and
Data Assimilation Office, NASA Goddard Space Flight Center,
Greenbelt, Maryland

Robert Atlas
Data Assimilation Office, Laboratory for Atmospheres,
NASA Goddard Space Flight Center, Greenbelt, Maryland

[1]Corresponding author's address: NASA Goddard Space Flight Center, Code 910.3, Greenbelt, MD 20771, Email oreale@dao.gsfc.nasa.gov

Abstract

The Mediterranean Sea region is dominated by baroclinic and orographic cyclogenesis. However, previous work has demonstrated the existence of rare but intense subsynoptic-scale cyclones displaying remarkable similarities to tropical cyclones and polar lows, including, but not limited to, an 'eye-like' feature in the satellite imagery. The terms polar low and tropical cyclone have been often used interchangeably when referring to small-scale, convective Mediterranean vortices and no definitive statement has been made so far on their nature, be it sub-tropical or polar. Moreover, most of the classifications of Mediterranean cyclones have neglected the small-scale convective vortices, focusing only on the larger-scale and far more common baroclinic cyclones.

A proposed classification of all Mediterranean cyclones based on operational global analyses is the outcome of this article. The classification is based on normalized horizontal shear, vertical shear, scale, low versus mid-level vorticity, low-level temperature gradients, and sea surface temperatures. In this classification system there is a continuum of possible events, according to the increasing role of barotropic instability and decreasing role of baroclinic instability. One of the main results is that the Mediterranean tropical cyclone-like vortices and the Mediterranean polar lows appear to be different types of events, in spite of the apparent similarity of their satellite imagery. A consistent terminology is adopted, stating that tropical cyclone-like vortices are the less baroclinic of all, followed by polar lows, cold small-scale cyclones and finally baroclinic lee cyclones. This classification is based on all the cyclones which occurred in a four-year period (between 1996 and 1999). Four cyclones, selected among all the ones which developed during this time-frame, are analyzed. Particularly, the classification allows to discriminate between two cyclones (occurred in October 1996 and in March 1999) which both display a very well-defined "eye-like" feature in the satellite imagery. According to our classification system, the two events are dynamically different and can be categorized as being respectively a tropical cyclone-like vortex and well-developed polar low.

1 Introduction

1.1 Previous work

This article aims to organize the existing information on Mediterranean cyclones in a simple, dynamically-based classification including all the types of cyclones that have been observed over the Mediterranean region between 1996 and 1999.

The need for a comprehensive classification arises because previous attempts to classify Mediterranean cyclones have been based only on the climatology of baroclinic and orographic cyclones (e.g., Alpert et al 1990; Trigo et al. 2002). However, in the Mediterranean there is also strong evidence of small-scale convective vortices, similar to tropical cyclones and polar lows: a number of case studies on individual storms exists in the literature (e.g. Pytharoulis et al. 1999). No attempt has been made so far to include this kind of events into a comprehensive classification of Mediterranean cyclones.

The starting point of this work is a previous article by Reale and Atlas (2001), hereafter referred to as RA01. RA01 open with a literature review of the so-called Mediterranean cyclogenesis, stating that at least three different types of cyclones have been documented by previous authors in the Mediterranean region: 1) baroclinic-lee cyclones (Buzzi and Tibaldi 1978; McGinley 1982; Speranza et al. 1985; Buzzi and Speranza 1986); 2) sub-synoptic scale vortices resembling tropical cyclones and polar lows (Ernst and Matson 1983; Billing et al. 1983; Mayengon 1984; Rasmussen and Zick 1987; Businger and

Reed 1989; Blier and Ma 1997; Pytharoulis et al. 1999) and 3) cold small scale cyclones (so defined by Alpert and Neeman 1992) that seem to be an intermediate category between the last two.

Then, RA01 analyze two cyclones that developed over the western-central Mediterranean on 3-6 October 1996 and 7-10 October 1996 and noted a similarity with those tropical storms that develop outside of the tropical environment, or in proximity of a baroclinic environment. We will refer to these storms as to 9610A and 9610B. The storm 9610A had an early landfall over Sicily and Calabria (southern Italy), and produced accumulated rainfall of 480.4 mm at Santuario di Polsi (southern Calabria). The storm 9610B tracked mostly over the sea and could develop a very compact and distinct eye-like feature (RA01, Figures 9 and 12). Measures in the storm center are not taken operationally in the Mediterranean; however, wind observations at about 100 km from 9610's center indicate wind speeds well above the tropical storm intensity threshold (RA1, Figures 10e and 13c,d) and damages due to wind on the Aeolian islands suggest that wind speed of hurricane-level intensity ($32\ m\,s^{-1}$) was reached. The most important findings in RA01 are:

1. The National Centers for Environmental Predictions (NCEP) operational analyses are a valid tool to detect the "signature" of tropical cyclone-like vortices. The analyses, although limited by the $1^o \times 1^o$ horizontal resolution, are consistent with the surface observations, satellite imagery and Special Sensor Microwave Imager (SSM/I) data.

2. During the entire life-time of the storm, the vertical shear (calculated as the difference in wind speed between 300 hPa and 850 hPa) is virtually zero over the center of the cyclone, indicating that baroclinicity at the storm scale is negligible, even though the surrounding environment is baroclinic (RA1, Figure 21).

3. During the storm development and intensification the zonal component of the wind at 700 hPa, above the surface center, satisfies Kuo's necessary condition for barotropic instability (RA1, Figure 22).

Point 1 enables us to attempt a classification of cyclones based on the NCEP analyses. Points 2 and 3 contrast with previous works on polar lows, where barotropic instability is in general regarded as unimportant, and baroclinic instability as necessary in the lower levels (Sardie and Warner 1983; Businger and Reed 1989). This discrepancy however, could be solved if the storms 9610A and 9610B were not polar lows. On this issue, the terminology adopted by various authors is very confusing because the terms 'tropical' and 'polar low' have been used very freely. For example, Businger and Reed (1989) thought that all Mediterranean meso-cyclones are "cold-low type" polar lows, but other authors referred to one case of a convective vortex that occurred in January 1995 as to a 'Mediterranean Sea hurricane' (Blier and Ma 1997), or 'hurricane-like cyclone' (Pytharoulis et al. 1999).

1.2 Different types of cyclones

The main task of this paper is to organize the large, somewhat contradictory set of information on Mediterranean cyclones, providing a classification and a more rigorous terminology to discriminate about different cases. Particularly, a more restrictive definition of polar low and tropical cyclone-like vortex is searched. To do so, all the cyclones which occurred between 1996 and 1999 over the Mediterranean have been analyzed. Only moderate or intense systems lasting at least twelve hours have been considered. For each cyclone, normalized horizontal shear at 700 hPa above the surface center, vertical shear above the surface center, 850 hPa vorticity, 500 hPa vorticity, 850 hPa temperature gradients have been calculated. For each cyclone, it was checked if Kuo's barotropic instability condition for the zonal component of the flow at all levels between 850 and 300 hPa is verified or not. Moreover, the following factors have also been looked at: symmetry, satellite imagery and sea surface temperatures (SSTs). Comparison with conventional observations was performed for each individual cyclone.

The outcome of this work of evaluation is a set of objective criteria which allows to classify all the cyclones that have been observed during this time-frame. According to our findings, polar lows (hereafter PLs) and tropical cyclone-like vortices (hereafter TCLVs) both occur in the Mediterranean but appear to be different kind of events, even though the satellite imagery is similar. Some discriminating factors which allow to distinguish the storm

9610B (which we will classify as a TCLV) from polar lows will be outlined. Namely, only the storm 9610B simultaneously satisfies the necessary conditions for barotropic instability across all levels above the center, displays values of vertical shear about zero (or slightly negative) over the storm center, and occurs over an area where latent heat flux dominates over sensible heat flux, the former being from three to five times larger than the latter.

Three cases of highly representative Mediterranean cyclones, among all of those observed in the 1996-99 period, are selected, to be compared with cyclones 9610A and 9610B. These storms occurred in April 1997, November 1997 and March 1993 and will be named as 9704A, 9711A, 9903B. The naming convention is the same adopted in RA01 for the 9610A and 9610B storms (2 digit year and month number, followed by a letter of occurrence in that month). Each of these cyclones is selected due to the fact that it might present some superficial similarity with the event 9610B: in fact, two of them display a more or less pronounced an eye-like feature and all of them have some degree of alignment between geopotential minima at all levels. The storm 9704A is an intense baroclinic cyclone close to the occlusion stage; the second (9711A) is a convective smaller scale cyclone and the third (9903B) is even smaller and has an extremely well-defined spiral structure and a very distinct eye-like feature. The signatures in the gridded analyses relative to the storms 9610A and 9610B are compared with the signatures of cyclones 9704A, 9711A and 9903B. According to the criteria stated in this work, it

will be shown that no ambiguity exists among them: none of these storms is a TCLV as the cyclone 9610B, and the cyclone 9903B can be classified as a well-developed PL.

The result is thus a new classification of cyclones, based on eleven conditions, among which scale, structure and causative mechanisms. This classification is comprehensive of all cyclones that were observed between 1996 and 1999. The general set of criteria provided by this work can be easily implemented into an automated diagnostic of gridded analyses (or forecast), allowing a forecaster to distinguish the signature of tropical cyclone-like vortices, (like the storm 9610B) from the signature characterizing PLs, cold small scale cyclones (hereafter, CSCs) and intense occluded baroclinic lee cyclones (BLCs).

2 Barotropic instability

2.1 Previous studies

The necessary condition for barotropic instability to occur in a zonal flow varying with latitude and time $U(y,t)$, having no vertical shear (i.e., in a barotropic atmosphere) and a nonzero meridional velocity shear $\frac{\partial U}{\partial y}$, symmetrical with respect to a certain latitude, in a linear theory framework, is (Kuo 1949):

$$\beta - \frac{\partial^2 U}{\partial y^2} = 0 \tag{1}$$

Nitta and Yanai (1969) analyzed the barotropic instability of two idealized westerly and easterly jets:

$$U_W = U_{max} sin^2 \frac{\pi y}{2b} \tag{2}$$

$$U_E = -U_{max} sin^2 \frac{\pi y}{2b} \tag{3}$$

where b is the half-width of the jet. Their main result is a family of critical curves, which provides the growth rate for a wave of wavelength L, extracting energy from that flow, for each given L/b and jet intensity U_{max}.

Based on these results, it has been generally agreed that horizontal shear, and therefore barotropic instability, cannot be considered a cause for the development of polar lows. The main reason is that it was believed that horizontal velocity gradients in jets are not sharp enough to develop wavelengths as small as the scale of polar lows. Sardie and Warner (1985) and Businger and Reed (1989) concluded that, given what they thought was a strong shear for a westerly jet (i.e, 80 $m\,s^{-1}$ over 500 km) the corresponding growth rate would be too small. Therefore, Sardie and Warner (1985) stated that both moist baroclinicity and CISK are concurring causative mechanisms for the northern Atlantic polar lows, pointing out the need of a strong vertical shear into the lower levels.

However, in RA01 it is shown that the vertical shear is virtually zero over the developing low and the horizontal shear is substantially stronger than the one considered by Sardie and Warner. These conclusions deserve further discussion.

2.2 Analysis of the horizontal shear at 700 hPa

In the northern hemisphere, cyclonic shear exists wherever the meridional derivative of the zonal wind is negative, i.e., on the southerly side of an easterly jet and on the northerly side of a westerly jet. However, cyclonic shear exists also wherever the zonal derivative of the meridional wind is positive, i.e., on the easterly side of a northerly jet and on the westerly side of a southerly jet. This contributions could be important for small wavelengths in the mid-latitudes, although, because of its complexity, the subject of non-zonal flow is not frequently discussed in theoretical studies: a treatment of instability of on arbitrarily oriented flow or of a curved flow is given in Grotjahn (1981) and Grotjahn (1983).

We start analyzing the cyclonic shear at 700 hPa relatively to the storm 9610B. In Figure 1 the opposite of the 700 hPa meridional derivative of the zonal wind, the 700 hPa zonal derivative of the meridional wind and their sum, all scaled by the local Coriolis parameter $f(y)$

$$-\frac{1}{f(y)}\frac{\partial u}{\partial y};\ \frac{1}{f(y)}\frac{\partial v}{\partial x}\ and\ \frac{1}{f(y)}(\frac{\partial v}{\partial x}-\frac{\partial u}{\partial y}) \tag{4}$$

are displayed against the sea level pressure. They are an indication of cyclonic shear generated by the zonal and meridional components of the wind, and by the total wind. The latter is a non-dimensional, normalized relative vorticity. To display the cyclonic shear in a non-dimensional normalized manner suggests how effective a certain shear is, given the environment.

At 12 UTC 6 October 1996, by the start-up of the cyclogenetic process, the the total 700 hPa relative vorticity is greater than $1f$ over the western side of the developing low (Figure 1a).

At 00 UTC 7 October 1996, the horizontal shear of the 700 hPa zonal wind approximately doubles the shear of the meridional wind (Figure 1b), but their total becomes perfectly symmetric with respect to the surface low.

Twelve hours later, at 12 UTC 7 October 1996, the storm begins to display a spiral structure. The 700 hPa shear of the zonal wind is still twice the shear of the meridional wind, but the total shear increases becoming greater than $2f$ right over the storm center (Figure 1b). The total 700 hPa shear remains larger than $2f$ at 00 UTC 8 October 1996 (Figures 1d), although at this time the contributions to the shear generated by the meridional wind $\frac{\partial v}{\partial x}$ and by the zonal wind $-\frac{\partial u}{\partial y}$ are of the same magnitude. The symmetry of the total scaled relative vorticity with respect to the surface low, and the equivalent size of the zonal and meridional components, can still be observed at 12 UTC 8 and 00 UTC 9 October 1996 (Figures 1e,f)

It is noteworthy to observe that the area over which the total horizontal shear at 700 hPa is greater than $2f$ at 12 UTC 7 October and 00 UTC 8 October 1996, perfectly corresponds with the surface minimum position and with the area over which the vertical shear between 300 hPa and 850 hPa is small or even slightly negative (RA01, Figures 21c,d).

2.3 Verification of the Kuo necessary condition

For each longitude x, the function

$$K(y) = \frac{\partial}{\partial y}\Big(f(y) - \frac{\partial U}{\partial y}\Big) \tag{5}$$

represents the meridional variation of the difference between the local Coriolis parameter and the vorticity generated by the zonal component of the wind. The areas where $K(y) = 0$ are the ones in which barotropic instability is not impossible, in response to the shear of the zonal component of the flow. Figure 2 shows that, as already seen in RA1, the necessary condition for barotropic instability to occur is satisfied at 700 hPa above the surface center for the storm 9610B. The storm center is always located to the north of a maximum and to the south of a minimum of $K(y)$, with values very close to zero.

However, for this particular storm, the Kuo necessary condition for barotropic instability is satisfied not only at 700hPa, but also in the upper levels, above the storm center. Meridional cross-sections of the magnitude of the total wind and of $K(y)$, are displayed together in Figure 3. The correspondence of the eye-like feature (inferred by the low-speed cylinder), with an axis along which

$$\frac{\partial}{\partial y}\Big(f(y) - \frac{\partial U}{\partial y}\Big) = 0 \tag{6}$$

is noteworthy. At 12 UTC 6 October 1996, when the storm is at its onset, the vortex, characterized by low speed values and $K(y) = 0$ along its axis,

is initially centered at 38^0N and 5^0E and is quite shallow: from the surface up to 750 hPa. But for as long as the evolution of the storm progresses, the necessary condition for barotropic instability becomes satisfied throughout a gradually deeper layer. At 00 and 12 UTC 7 October 1996 the line defined by $K(y) = 0$ goes up to 500 hPa, (Figures 3b,c) and at 00 UTC 8 October 1996 extends up to 300 hPa (Figure 3d).

3 Towards a classification of Mediterranean cyclones

A classification of the different kinds of cyclones observed in the Mediterranean was first attempted by Alpert et al. (1990), using ECMWF 2.5^0 resolution data and an objective method to define, select and track the cyclones. Their approach appears useful for the baroclinic cyclones, but for the scales involved in the 9610A and 9610B storms, and for the cyclones described in Billing et al., (1983), Ernst and Matson (1983), Mayengon (1984), Rasmussen and Zick (1987), Blier and Ma (1997), the 2.5^0 resolution data are too coarse.

In RA01 it was demonstrated that $1^o \times 1^o$ NCEP gridded analyses, given the resolution limit, completely confirm the observational evidence of conventional data, stationary infrared and visible imagery and SSM/I data, thus allowing the detection of what can be called the '1^o signature' of tropical-like cyclogenetic processes. This signature is also evident in other models at com-

parable resolutions: studies on similar cyclones have been performed with the finite volume model and data assimilation system (fvDAS) currently adopted at the National Aeronautics and Space Administration, Data Assimilation Office, providing comparable or better representations of these storms (not shown).

Therefore, we believe that there is some foundation to attempt a classification of all the Mediterranean cyclones using $1^o \times 1^o$ or higher resolution data. This is particularly important considering that even in very recent times, an article aiming to classify Mediterranean cyclogenetic mechanisms (Trigo et al. 2002) with the aid of 1.125×1.125^o data, does not include or even mention Mediterranean tropical cyclone-like vortices or Mediterranean polar lows.

In our study, all the cyclones, (not only the baroclinic and orographic ones) occurred in the Mediterranean between 1996 and 1999 were analyzed with the aid of the NCEP operational analyses. Only moderate or intense systems have been considered: more precisely, the cyclones 1) characterized by at least two closed contours in the sea level pressure field (with a contour interval of 2 hPa) and 2) appearing for at least three consecutive time-steps (12 hours) in the analyses. The following quantities have been calculated for each cyclone: normalized horizontal shear above the surface center at 700 hPa, verification (or not) of the Kuo barotropic instability condition for the zonal component of the flow across the entire column of atmosphere between

850 and 300 hPa above the surface center, vertical shear above the surface center, 850 hPa vorticity, 500 hPa vorticity, 850 temperature gradients. Moreover, the following factors have also been looked at: symmetry, satellite imagery (presence of a comma-cloud, spiral structure and of an eye-like feature) and sea surface temperatures (SSTs). Comparison with conventional observations was performed for each individual cyclone.

All this information is condensed into Table 1. We propose to classify all the cyclones as a sequence of events in which the similarity with tropical cyclones increases going from left to right. We also decide to categorize these events only for their dynamical differences, rather than relating them to location in which they form. In this sense, we wish to create a classification which is not geographically dependent. One can observe that:

- The scale and the role played by baroclinic instability (measured as the 300-850 hPa wind shear and as temperature gradients at 850 hPa) and by mid-tropospheric vorticity, decreases from left to right.

- The role played by barotropic instability (seen as horizontal shear at 700 hPa, verification of Kuo's condition for barotropic instability at 700 hPa over the surface center and vertically across all the tropospheric levels above the center), and also symmetry, evidence of a warm thermal core, low-level vorticity and SST, increase from left to right.

In this continuum frame, some arbitrarily chosen separations can be adopted: we decide to place them using the existing terminology. So, we distinguish,

from left to right, baroclinic lee cyclones, cold small scale cyclones, polar lows and tropical cyclone-like vortices.

It is worth observing that all the cyclones that result being classified as BLCs and CSCs in our system, do not have an eye-like feature but might occasionally display a comma-cloud. The storms that result categorized as PLs always have a comma-cloud and occasionally an eye-like feature when they are very well-developed; TCLVs always have an eye-like feature.

The information condensed in Table 1 is sufficient to categorize in a unique way all the cyclones occurred between 1996 and 1999 in the Mediterranean region, as they appear in the gridded 1^o NCEP operational analyses. We believe that the criteria stated in Table 1 can be applied to any set of operational analyses, and can easy be implemented in an objective system which can allow forecasters to categorize any type of cyclone associating a certain level of risk.

An important observation is that, from the available observations, the 9610A cyclone did not seem to reach the hurricane-level wind speed threshold like 9610B, possibly because of early landfall (RA01, Figures 4a,b,c,d); nevertheless, the rainfall produced by 9610A is comparable with the one detected during some major hurricane landfall (RA01, Figures 4e,f): up to 480 mm were recorded over southern Calabria. The Mediterranean is filled with severe flood cases, with precipitation rates on the order of 500 mmd^{-1}. Recent examples are the November 1994 floods (Krichak and Alpert 1998).

The November 1994 and many other Mediterranean floods are related with large-scale transport of moisture from tropical latitudes (Krichak and Alpert 1998, Reale et al 2002) and the weather systems that use that anomalous excess of moisture to produce the actual flood can often be a moderate or even weak baroclinic cyclone. However, it is not unreasonable to speculate that, in the past, not fully developed sub-synoptic scale convective vortices similar to 9610A, possibly nested within a larger scale baroclinic environment, could have escaped forecasters' and analysts' eyes because of poor resolution and lack of observational data, and might have enhanced or contributed to some of the disastrous floods.

Statistical analysis of precipitation data in Italy reveals the presence of two precipitation "modes": one of the two, called 'extraordinary', is characterized by exceptional precipitation rates and very rare occurrence (Rossi et al. 1984a,b; Furcolo et al. 1998). The return period on a local scale of these outliers is very large, but on a regional scale these events seem to be very important. Two-Component Extreme Value analyses for flood frequency reveals that, in Italy, the probability that the annual maximum of precipitation and/or stream-flow comes from an extraordinary event is about 26% (Fiorentino et al., 1987), whereas for another mid-latitude region, e.g. Great Britain, the same probability is evaluated around just 3% (Rossi et al., 1986). This result might be indirect evidence that TCLVs are not uncommon in the Mediterranean on a regional scale. If so, their prompt detection

could perhaps be an important step towards more appropriate strategies for damage mitigation.

4 Examples of a BLC and PLs

4.1 The cyclone 9704A

Some examples of different cyclones are now analyzed with the criteria described in Table 1. The first case, which will be referred to as 9704A, is a BLC at its peak of intensity. It was chosen because in a baroclinic cyclone close to the occlusion the upper level cutoffs can almost be aligned with the surface minimum. However, it will be shown that the vertical structure is represented very differently in the analyses, with respect to the storm 9610B.

In Figures 4a,b the sea level pressure and the 500 hPa geopotential at 12 UTC 21 April 1997 (data to the south of 34^0N and to the west of 10^0W are not saved), are displayed. The cyclone originated in the southwestern Mediterranean on April 20 and had almost explosive development. By the 12 UTC 21 April 1997 the maximum deepening was reached, and the surface center became almost aligned with the upper level cutoff. The first difference with respect to the storm 9610B is the much larger scale, as it will be shown later in the satellite image. Another important difference appears in Figure 4c: the surface center of cyclone 9704A is not placed under a maximum of the 700 hPa non dimensional vorticity. Conversely, in the cyclone 9610B, the surface sea level pressure minimum was right under an area in which the

700 hPa ($\frac{\partial v}{\partial x} - \frac{\partial u}{\partial y}$) exceeded $2f$ (Figure 1). The analysis of the 300 minus 850 hPa wind velocity highlights the difference. In RA01 (Figures 18c,d) it was shown that the storm 9610B developed within an area of negligible or slightly negative vertical shear (approximately $-5\ m\,s^{-1}$). On the other hand, the cyclone 9704A, even being at a phase close to occlusion, still displays strong positive values of vertical shear on the eastern side, up to 35 $m\,s^{-1}$. Even in proximity of the storm center, two positive maxima greater than 5 $m\,s^{-1}$ can be seen. Figures 4e,f show the wind at 300 hPa and 500 hPa. A comparison with the storm 9610B (RA01, Figures 17 and 18a,b) reveals that, for the cyclone 9704A, the upper level winds are stronger in proximity of the storm center. Satellite imagery (Figure 5) displays a typical Mediterranean baroclinic cyclone at an occluding stage. The scale spans almost from Gibraltar to Greece, and the difference with the very small vortex 9610B at its peak of intensity (RA01, Figures 12a,b) is evident. The vertical structure is shown in Figures 6a,b. The alignment of the cutoffs at all levels with the surface center, typical of the occluding systems, allows the existence of a broad low wind speed cylinder in the storm center (Figures 6a,b). However, in spite of the alignment, the temperature fields still display strong baroclinicity up to 500 hPa, evident warm and cold advection in the meridional cross-section, and no evidence of a warm core. Particularly, the 5^0C isotherm in the zonal cross-section falls from 700 hPa to the east of the storm to 900 hPa to the west (Figure 6a). Similarly, the meridional cross-section displays a drop of

almost 200 hPa in the 0^0C isotherm going from south to north across the storm center. Cross-sections at an earlier stage of the cyclone 9704A obviously display even stronger temperature variations across the storm (not shown), with even more dramatic slope in the isotherms. Conversely, the cross-sections across the storm 9610B (RA01, Figures 14 and 15) and across the named tropical storm Josephine which was displayed in RA01 for comparison (RA01, Figure 16), reveal much weaker baroclinicity.

4.2 The cyclone 9711A

At 13:59 UTC and 17:36 UTC 23 November 1997, the NOAA polar orbiter satellite displays a cyclone (Figures 7a,b) somewhat similar to the storm 9610A (RA01, Figures 3a,b), although characterized by a lower degree of organization. Figures 8a,b show the alignment between the surface center and the corresponding 500 hPa cutoff at 00 UTC 24 November 1997. Figure 8c shows the 700 hPa horizontal wind shear, scaled by the local Coriolis parameter. There is an area close to the surface low, in which $(\frac{\partial v}{\partial x} - \frac{\partial u}{\partial y})_{p=700hPa} is about 2f$. However, the symmetry is not comparable with the storm 9610B. The vertical 300-850 hPa wind shear reveals a large area of negligible vertical shear over the surface low (Figure 8d), but the surface center does not correspond to the area where the vertical shear is negative, as was the case for the 9610B storm (RA01, Figures 21c,d). The 300 and 500 hPa wind displays a tight loop over the surface low, with noticeable horizontal shears (Figures 8e,f). The cross section across the storm center shows a

low-speed cylinder and negligible baroclinicity, but there is no evidence of a centered warm core (Figure 9).

4.3 The cyclone 9903B

At 2:33 27 March 1999 the NOAA polar orbiter satellite displays a cyclone with a distinct and very well-defined eye-like feature which would resemble a 'tropical' cyclone (Figure 10).

However, the criteria of classification we propose would reveal this cyclone to be rather a well-developed polar low. Figures 11a,b show a surface cyclone and its corresponding cutoff; its small scale is comparable to the event 9610B. However, Figure 11c shows that the normalized 700 hPa vorticity scaled by the local Coriolis parameter ($\frac{\partial v}{\partial x} - \frac{\partial u}{\partial y}$) exceeds $1f$, but it does not reach $2f$. In good correspondence with the surface low, an area of negative vertical shear is evident in Figure 11d. The 300 and 500 hPa wind display a very tight loop over the surface low, with noticeable horizontal shears (Figures 11e,f). The cross section across the storm center reveals the expected low-speed cylinder, a substantial low-level wind maximum and an evident sloping warm core in both the zonal and meridional cross-sections (Figures 12a,b).

However, substantial baroclinicity in the lower levels, revealed by the slope of the isotherms, is the important difference with the vertical sections across cyclone 9610B (RA01, Figures 14 and 15). Conversely, this factor represents a strong similarity with polar lows in which, according to Sardie and Warner (1985), low-level baroclinicity must be present.

4.4 Classification of cyclones 9704A, 9711A, 9903B

To strengthen our understanding of these cyclones's similarities and differences, the Kuo necessary condition for barotropic instability is analyzed.

The center of the storm 9610A corresponds to an area where the 700 hPa $K(y)$ is close to zero; the meridional vertical section reveals that $K(y) = 0$ throughout almost the entire troposphere above the surface low (Figures 13a,c).

Conversely, $K(y) = 0$ for the cyclone 9704A at 700 hPa, but not throughout the troposphere: the meridional vertical section reveals that the Kuo condition for barotropic instability is satisfied only up to 650 hPa (Figures 13b,d).

Kuo's necessary condition for barotropic instability is satisfied for both the storms 9711A and 9903B (Figures 14a,c;b,d). 9903B however, as seen in Figures 9 and 12, reveals some baroclinicity in the lower levels. To further investigate this aspect, the horizontal temperature gradients at the 850 hPa level, displayed over the sea level pressure field, are shown in Figure 15 for all the cases.

It appears evident that the smaller and the less baroclinic of all the storms examined is the 9610B event, here displayed at two different stages: 12 UTC 7 October 1996 and 12 UTC 8 October 1996 (Figures 15b,c). The storm 9711A also has negligible baroclinicity at 850 hPa (Figure 15e). Some baroclinicity as manifested by warm advection is present to the south of the storm 9610A

(Figure 15a). Stronger temperature gradients, due to both cold and warm advection to the northwest and to the southeast of storm 9903B, are evident in Figure 15f. The cyclone 9704A, as expected, is the most baroclinic of all the storms we analyzed: in spite of being at an occluding stage, 850 hPa temperature gradients to the north of the center, due to cold advection, are of about 4^0C over 100 km.

Considering all these factors, and recalling from RA01 that SST values range from 21^oC to 26^oC during 9610A and 9610B development, whereas SSTs are much lower in the 9704A, 9711A and 9903B cases (ranging from $10^o - 12^oC$ during the 9903B development, to about $18^o - 21^oC$ in the 9711A case, not shown), it can be concluded that Table 1 characterizes without ambiguity all the cyclones previously examined. We could define therefore 9704A a case of an intense BLC and 9903A as a polar low. The only storm that satisfies all the criteria to be a tropical cyclone-like vortex is 9610B. The cyclone 9711A appears a transition between a PL and a TCLV, and the 9610A could be defined as a non-fully developed TCLV, due to an early landfall (recall RA01).

The criteria defined in Table 1 are suggestive that winter hurricane-like vortices, like the ones observed in the central Mediterranean in January 1982 (Billing et al., 1983; Ernst and Matson 1983; Businger and Reed 1989) and in January 1995 (Blier and Ma 1997) are polar lows. In the latter case, SSTs were recorded in most violent part of the storm by the German ship

Meteor, and ranged from 16^0C to 20^0C, whereas air temperature was of about 7^0C (data from Deutsche Wetterdienst). Numerical simulations done by Pytharoulis et al. (1999) on this particular case reveal the role of sensible heat to be of the same magnitude of the latent heat, in agreement with other studies on polar lows outside the Mediterranean, and in contrast with tropical cyclones, where latent heat flux is more important than sensible heat flux. Conversely, RA1 showed the observed SSTs relative to 9610A and 9610B (ranging from $21°C$ to $26°C$) and calculated the corresponding values of latent heat and sensible heat based on ship observations, coming to the conclusion that, for both storms, latent heat flux was three to five times larger than sensible heat.

All these findings are consistent with the fact that the temperature difference between air and sea, (and therefore sensible heat flux) is larger in winter, and SST (and therefore latent heat flux) is is higher in early fall. This further supports the idea that the Mediterranean winter convective vortices are different from the events occurring in September and October like the storms 9610A and 9610B.

5 Conclusions

This work is the continuation of a previous article by Reale and Atlas (2001). The main goal is to demonstrate that a variety of events can occur over the Mediterranean region, ranging from purely baroclinic to tropical cyclone-

like vortices. In this work we provide a set of eleven criteria, condensed in Table 1, that should allow operational forecasters to use gridded analyses (or forecasts) to discriminate between different types of cyclones.

Before this work, the terms polar low and tropical cyclone-like vortices have been often used interchangeably to refer to Mediterranean cyclones displaying an eye-like feature in the satellite imagery. One of the outcomes of this work is to show that, in spite of their apparent similarity in the satellite imagery, Mediterranean polar lows and Mediterranean tropical-cyclone like vortices are represented differently in gridded analyses and should be conceived as different types of storms.

The absence of low-level baroclinicity at the storm scale and the crucial role played by barotropic instability is the key factor that allows us to distinguish the 7-10 October 1996 cyclone, which we define as tropical cyclone-like vortex, from the 27 March 1999 event, which we classify as a polar low. Particularly, the latter event appear to be fully consistent with some of the attributes that previous authors have verified in polar lows, namely a cooperative interaction of baroclinic instability and air-sea fluxes, with the presence of substantial low-level temperature advection.

Acknowledgments The initial part of this work was done at the Center for Ocean-Land-Atmosphere Studies (COLA), Calverton, Maryland, and was supported by the Centro Interuniversitario di Ricerca in Monitoraggio Ambientale (CIMA), University of Genoa, Italy, under a cooperative agreement for the improvement of precipitation forecasts in the Western Mediterranean region. The NOAA satellite imagery is a courtesy of the Dundee Satellite Receiving Station, Dundee University, Scotland. The METEOSAT images (courtesy EUMETSAT) are provided by the University of Nottingham, UK. We wish to thank Juan Carlos Jusem and Austin Conaty for helpful suggestions.

REFERENCES

Alpert, P., B. U. Neeman and Y. Shay-El, 1990: Climatological analysis of Mediterranean cyclones using ECMWF data. *Tellus,* **42A,** 65-77.

Alpert, P. and B. U. Neeman, 1992: Cold small-scale cyclones over the eastern Mediterranean. *Tellus,* **44A,** 173-179.

Billing, H., I Haupt and W. Tonn, 1983: Evolution of a hurricane-like cyclone in the Mediterranean Sea. *Beitr. Phys. Atmos.,* **56,** 508-510.

Blier, W. and Q. Ma, 1997: A Mediterranean Sea Hurricane? *UCLA Tropical Meteorology Project Newsletter,* **12,** 15a.8

Businger, S. and R. J. Reed, 1989: Cyclogenesis in Cold Air Masses, *Wea. Forecasting,* **4,** 133-156.

Buzzi, A. and S. Tibaldi, 1978: Cyclogenesis on the lee of the Alps: a case study. *Q. J. R. Met. Soc.* **104,** 271-87.

Buzzi, A. and A. Speranza, 1986: A theory of deep cyclogenesis in the lee of the Alps. Part II: Effects of finite topographic slope and height. *J. Atmos. Sci.,* **43,** 2826-2837.

Ernst, J. A. and M. Matson, 1983: A Mediterranean tropical storm? *Weather,* **38,** 332-337.

Fiorentino, M., S. Gabriele, F. Rossi and P. Versace, 1987: Hierarchical approach for a regional flood frequency analysis. *Regional Flood Frequency Analysis,* D. Reidel Publ. Company, 35-49.

Furcolo, P., F. Rossi, and P. Villani, 1998: Analisi statistica della variabilità spaziale e temporale degli eventi estremi nelle regioni mediterranee (in Italian). *Tempeste mediterranee, CNR-GNDCI,* **Puble n. 1862,** 95-110.

Grotjahn, R. 1981: Stability properties of arbitrarily oriented mean flows. *Tellus,* **33,** 188-200.

Grotjahn, R. 1983: Stability properties of cylindrically curved mean flows. *Tellus,* **35,** 161-172.

Krichak, S. O. and P. Alpert, 1998: Role of large scale moist dynamics in November 1-5, 1994, hazardous Mediterranean weather. *J. Geoph. Res.,* **103,** 19453-19468.

Kuo, H. L., 1949: Dynamic instability of two-dimensional non-divergent flow in a barotropic atmosphere. *J. Meteor.,* **6,** 105-122.

Kuo, H. L., 1965: On the formation and intensification of tropical cyclones through latent heat release by cumulus convection. *J. Atmos. Sci.,* **22,** 48-63.

Mayengon, R., 1984: Warm core cyclones in the Mediterranean. *Mar. Wea. Log.,* **28,** 6-9.

Mc Ginley, J., 1982: Diagnosis of Alpine lee cyclogenesis. *Mon. Wea. Rev.*, **110,** 1271-87.

Nitta, T. and M. Yanai, 1969: A note on the barotropic instability of the tropical easterly current. *J. Meteor. Soc. Japan.* **47,** 127-130.

Ooyama, K. 1969: Numerical simulation of the life-cycle of tropical cyclones. *J. Atmos. Sci.,* **26,** 3-40.

Pytharoulis, I., G. C. Craig and S. P. Ballard 1999: Study of the Hurricane-Like Mediterranean Cyclone of January 1995. *Phys. Chem. Earth.* **24 B,** 627-632.

Rasmussen, E. and C. Zick, 1987: A subsynoptic vortex over the Mediterranean with some resemblance to polar lows. *Tellus,* **39 A,** 408-425.

Rasmussen, E. and C. Zick, 1989: A comparative study of tropical cyclones and polar lows. *Polar and Arctic Lows,* 47-80.

Reale, O. and R. Atlas 2001: Tropical Cyclone-like Vortices in the Extratropics: Observational Evidence and Synoptic Analysis. *Wea. Forecasting,* **16,** 7-34.

Reale, O., L. Feudale and B. Turato, 2001: Evaporative moisture sources during a sequence of floods in the Mediterranean region. *Geophysical Research Letters,* **28,** 2085-2088.

Reed, R. J., 1989: Cyclogenesis in polar air streams. *Mon. Wea. Rev.* **107,** 38-52.

Rossi, F., M. Fiorentino, P. Versace, 1984: Two-Component Extreme Value distribution for flood frequency analysis, *Water Resour. Res.,* **20,** 847-856.

Rossi, F., M. Fiorentino, P. Versace, 1984: Reply to the Comment on "Two-Component Extreme Value distribution for flood frequency anal-

ysis", *Water Resour. Res.,* **22,** 267-269.

Rotunno, R. and K. Emanuel, 1986: An Air-Sea Interaction Theory for Tropical Cyclones: Part II: Evolutionary Study Using a Nonhydrostatic Axisymmetric Numerical Model. *J. Atmos. Sci.,* **44,** 542-561.

Sardie, J. M. and T. T. Warner, 1983: On the mechanism for the devlopment of polar lows. *J. Atmos. Sci.* **40,** 869-881.

Sardie, J. M. and T. T. Warner, 1985: A numerical study of the development mechanism of polar lows. *Tellus,* **37,** 869-881.

Speranza, A., A. Buzzi, A. Trevisan and P. Malguzzi, 1985: A theory of deep cyclogenesis in the lee of the Alps. Part I. Modification of baroclinic instability by localized topography. *J. Atmos. Sci.,* **42,** 1521-1535.

Trigo, I., G. Bigg and T. Davies, 2002: Climatology of cyclogenesis Mechanism in the Mediterranean *Mon. Wea. Rev.,* **130,** 549-569.

Uccellini, L.W., R. A. Petersen, K. F. Brill, P. J. Kocin and J. J. Tuccillo, 1987: Synergistic interactions between an upper-level jet streak and diabatic processes that influence the development of a low-level jet and a secondary coastal cyclone. *Mon. Wea. Rev.,* **115,** 2227-2261.

	BLC	CSC	PL	TCLV
Scale km	500-1500	400-1000	300-600	300
Horizont. cyclonic shear $(1/f)/(\partial v/\partial x - \partial u/\partial y)$ at 700hPa	irrelevant	unimportant	concurrent > 1	crucial > 2
Kuo barotr. instability condition at 700hPa	can be satisfied	satisfied	always satisfied	always satisf.
Kuo barotr. instability condition across levels	not satisfied	partly satisf.	always satisfied	always satisf.
Baroclinic instability 300-850 hPa wind shear in ms^{-1}	crucial 30	crucial 25	important 10	inhibiting < -5
symmetry	asymmetric	quite symm.	symmetric	very symm.
thermal core	no core	cold core	sloping warm core nested in c.core	warm core
850 Vorticity s^{-1}	very low $< 10^{-5}$	low 10^{-5}	high 10^{-4}	maximum $> 1.2 \times 10^{-4}$
500 Vorticity s^{-1}	maximum $> 10^{-4}$	high 10^{-4}	low $< 10^{-4}$	quite low $< 0.5 \times 10^{-4}$
850 Temperature Gradients ${}^0C\ m^{-1}$	maximum $> 4 \times 10^{-5}$	large	small $< 2.5 \times 10^{-5}$	negligible $< 1.5 \times 10^{-5}$
SST	irrelevant	irrelevant	$< 21^0C$	$>\simeq 21^0C$

Table 1: Classification of Mediterranean cyclone based on NCEP operational analyses. BLC=baroclinic lee cyclone; CSC=cold small scale cyclone; PL=polar low; TCLV=tropical cyclone-like vortex. The involved variables, proceeding from top to bottom, are: 1) scale; 2) role played by horizontal shear, evaluated as the 700 hPa relative vorticity scaled by the local Coriolis parameter; 3) Kuo's necessary condition for barotropic instability at 700 hPa $(\beta(y) - \frac{\partial^2 U}{\partial y^2} = 0)$ over the surface center; 4) Kuo's necessary condition for barotropic instability across the entire column of atmosphere over the surface center; 5) baroclinic instability, evaluated as the 300 hPa minus 850 hPa wind shear; 6) symmetry; 7) presence of thermal cores; 8) 850 hPa vorticity; 9) 500 hPa vorticity; 10) 850 temperature gradients across the scale of the system; 11) SST. These values are calculated for cyclones occurred in 1996, 1997, 1998 and 1999.

Figure 1: Sea level pressure (hPa, continuous line), non-dimensional horizontal meridional shear of the 700 hPa zonal wind $-\frac{1}{f(y)}\frac{\partial u}{\partial y}$ (dotted line); non-dimensional horizontal zonal shear of the 700 hPa meridional wind $\frac{1}{f(y)}\frac{\partial v}{\partial x}$ (dashed line); at 12 UTC 6 Oct (a); 00 UTC 7 Oct (b); 12 UTC 7 Oct (c); 00 UTC 8 Oct (d); 12 UTC 8 Oct (e); 00 UTC 9 Oct (f). The two shadings represent areas where the 700 hPa non-dimensional total horizontal cyclonic shear $\frac{1}{f(y)}(\frac{\partial v}{\partial x} - \frac{\partial u}{\partial y})$ is greater than 1 (lighter) or 2 (darker). All non-dimensional quantities are scaled by the local Coriolis parameter.

Figure 2: Sea level pressure (hPa) and values of the function $K(y) = \frac{\partial}{\partial y}\left(f(y) - \frac{\partial U}{\partial y}\right)$ $(m^{-1}s^{-1})$, calculated at 700 hPa, at 12 UTC 6 Oct (a); 00 UTC 7 Oct (b); 12 UTC 7 Oct (c); 00 UTC 8 Oct (d); 12 UTC 8 Oct (e); 00 UTC 9 Oct (f). Contours at $2 \times 10^{-10}\ m^{-1}s^{-1}$. $K(y) = 0$ is the Kuo necessary condition for barotropic instability. The two shading represent areas where $K(y) < -10^{-10}$ (lighter) and $K(y) > 10^{-10}$ (darker).

Figure 3: Zonal vertical cross-sections of wind and $K(y)$ across the storm center at 12 UTC 6 Oct (a); 00 UTC 7 Oct (b); 12 UTC 7 Oct (c); 00 UTC 8 Oct (d). The magnitude of the total wind $(m\,s^{-1})$ is shaded; the values of $K(y)$ are contoured (contours every $2 \times 10^{-10}\ m^{-1}s^{-1}$). $K(y) = 0$ across the storm's axis.

Figure 4: Example of baroclinic cyclone (9704A) at 12 UTC 21 April 1997. Sea level pressure (hPa) (a); geopotential height at 500 hPa (m) (b); Sea level pressure (hPa) and total horizontal shear of the 700 hPa zonal wind, scaled by the local Coriolis parameter, $\frac{1}{f(y)}(\frac{\partial v}{\partial x} - \frac{\partial u}{\partial y})$; baroclinic shear (d), represented as in Alpert and Neeman (1992) as the difference in wind speed (ms^{-1}) between the 300 hPa and the 850 hPa levels; 300 hPa wind (e) and 500 hPa wind (ms^{-1}) (f). Data were not saved south of 34^0N and west of 11^0W.

Figure 5: Cyclone 9704A. METEOSAT satellite images in the infrared bandwidth at 12:00 UTC 21 Apr 1997: the scale of the cyclone spans from Gibraltar to the Balkans. Courtesy of EUMETSAT, through University of Nottingham, UK.

Figure 6: Cyclone 9704A. Vertical section of wind ($m\,s^{-1}$) and temperature (^0C) across the storm center at 39^0N (left) and at 9^0E (right) at 12 UTC 21 April 1997. Data were not saved above 200 hPa and south of 34^0N.

Figure 7: Example of meso-cyclonic vortex (9711A). NOAA satellite images in the infrared bandwidth. Courtesy of Dundee Satellite Receiving Station, Dundee University, Scotland. The storm center can be located to the east of Sicily at 13:59 (a) and at 17:26 (b) 23 November 1997.

Figure 8: Cyclone 9711A at 00 UTC 24 November 1997. Sea level pressure (hPa) (a); geopotential height at 500 hPa (m) (b); Sea level pressure (hPa) and total horizontal shear of the 700 hPa wind, scaled by the local Coriolis parameter, $\frac{1}{f(y)}(\frac{\partial v}{\partial x} - \frac{\partial u}{\partial y})$; baroclinic shear (d), represented as in Alpert and Neeman (1992) as the difference in wind speed (ms^{-1}) between the 300 hPa and the 850 hPa levels; 300 hPa wind (e) and 500 hPa wind (ms^{-1}) (f). Data were not saved west of 18^0W.

Figure 9: Cyclone 9711A. Vertical section of wind (ms^{-1}) and temperature (^0C) across the storm center at 38^0N (left) and at 17^0E (right) at 00 UTC 24 November 1997. Data above 200 hPa were not saved.

Figure 10: Example of meso-cyclonic vortex (9903B), which would result to be a polar low, according to our classification. NOAA satellite images in the infrared bandwidth. Courtesy of Dundee Satellite Receiving Station, Dundee University, Scotland. The storm center can be located to the west of Corsica at 2:33 27 March 1999. Notice the well-defined eye-like feature.

Figure 11: Cyclone 9903B at 00 UTC 27 March 1999. Sea level pressure (hPa) (a); geopotential height at 500 hPa (m) (b); Sea level pressure (hPa) and total horizontal shear of the 700 hPa wind, scaled by the local Coriolis parameter, $\frac{1}{f(y)}(\frac{\partial v}{\partial x} - \frac{\partial u}{\partial y})$; baroclinic shear (d), represented as in Alpert and Neeman (1992) as the difference in wind speed (ms^{-1}) between the 300 hPa and the 850 hPa levels; 300 hPa wind (e) and 500 hPa wind (ms^{-1}) (f). Data were not saved west of 18^0W.

Figure 12: Cyclone 9903B. Vertical section of wind (ms^{-1}) and temperature (^0C) across the storm center at 40^0N (left) and at 6^0E (right) at 00 UTC 27 March 1999. Data above 200 hPa were not saved.

Figure 13: Sea level pressure (hPa) and values of the function $K(y) = \frac{\partial}{\partial y}\left(f(y) - \frac{\partial U}{\partial y}\right)$ $(m^{-1}s^{-1})$, calculated at 700 hPa. Cyclone 9610A, at 12 UTC 4 Oct 1996 (a); cyclone 9704A, at 12 UTC 21 Apr 1997 (b). Contours at 2×10^{-10} $m^{-1}s^{-1}$. $K(y) = 0$ is the Kuo necessary condition for barotropic instability. The two shading represent areas where $K(y) < -10^{-10}$ (lighter) and $K(y) > 10^{-10}$ (darker).
Zonal vertical cross-sections of of wind and $K(y)$ across the storm center. Cyclone 9610A, at 12 UTC 4 Oct (c); cyclone 9704A, at 12 UTC 21 Apr 1997 (d). The magnitude of the total wind ($m\,s^{-1}$) is shaded; the values of $K(y)$ are contoured (contours every 2×10^{-10} $m^{-1}s^{-1}$). $K(y) = 0$ across the storm's axis.

Figure 14: Sea level pressure (hPa) and values of the function $K(y) = \frac{\partial}{\partial y}\left(f(y) - \frac{\partial U}{\partial y}\right)$ $(m^{-1}s^{-1})$, calculated at 700 hPa. Cyclone 9711A, at 00 UTC 24 Nov 1997 (a); cyclone 9903B, at 00 UTC 27 Mar 1999 (b). Contours at 2×10^{-10} $m^{-1}s^{-1}$. $K(y) = 0$ is the Kuo necessary condition for barotropic instability. The two shading represent areas where $K(y) < -10^{-10}$ (lighter) and $K(y) > 10^{-10}$ (darker).
Zonal vertical cross-sections of wind and $K(y)$ across the storm center. Cyclone 9711A at 00 UTC 24 Nov 1997 (c); cyclone 9903B at 00 UTC 27 Mar 1999 (d). The magnitude of the total wind ($m\,s^{-1}$) is shaded; the values of $K(y)$ are contoured (contours every 2×10^{-10} $m^{-1}s^{-1}$). $K(y) = 0$ across the storm's axis.

Figure 15: Sea level pressure (hPa) and magnitude of the 850 hPa temperature gradient ($^0C\ m^{-1}$). (a) cyclone 9610A at 12 UTC 4 October 1996; (b) and (c) cyclone 9610B at 12 UTC 7 October 1996 and 12 UTC 8 October 1996; (d) cyclone 9704A at 12 UTC 21 April 1997; (e) cyclone 9711A at 00 UTC 24 November 1997; (f) cyclone 9903B at 00 UTC 27 March 1999.

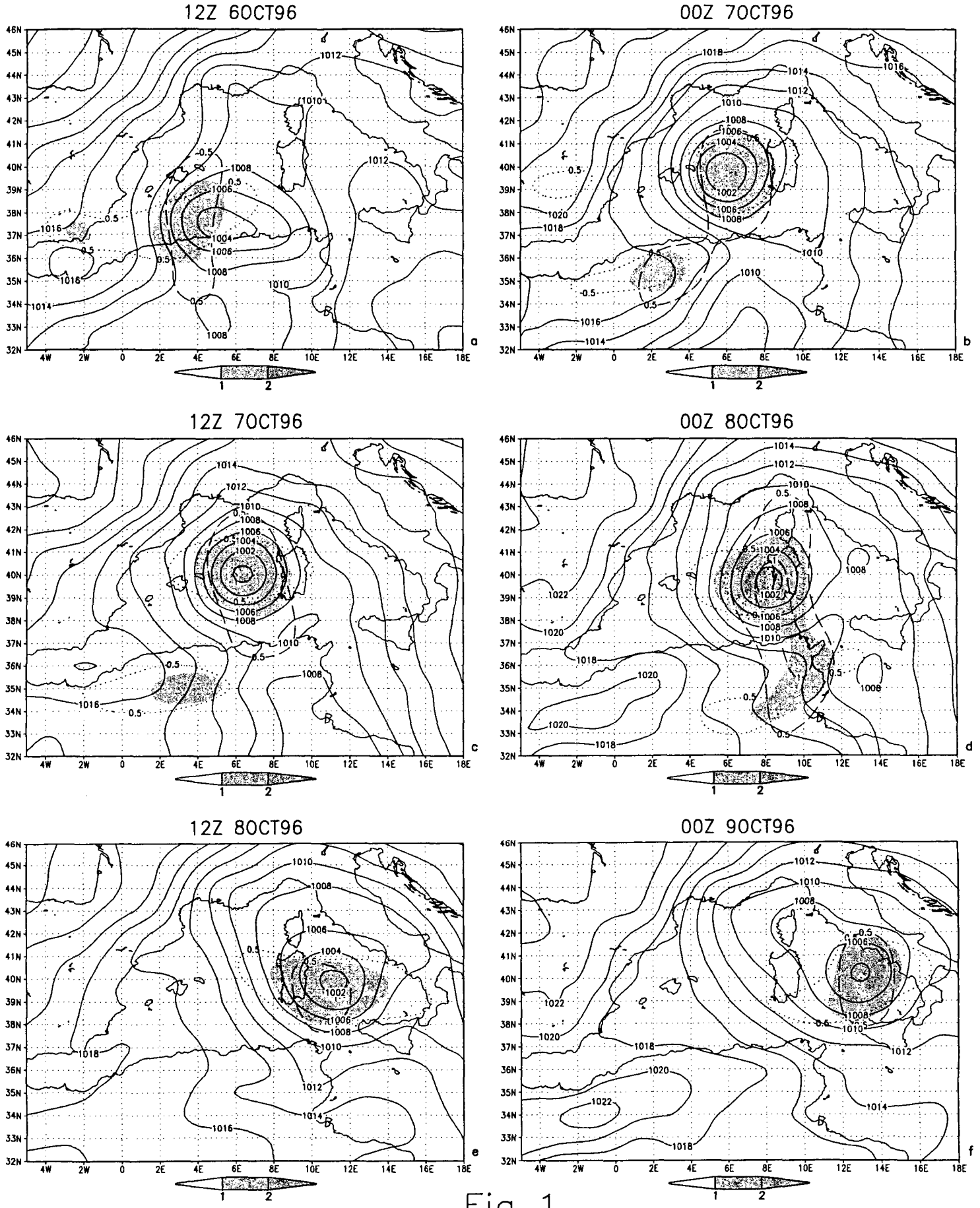
12Z 60CT96
00Z 70CT96
12Z 70CT96
00Z 80CT96
12Z 80CT96
00Z 90CT96
a
b
c
d
e
f

Fig 1

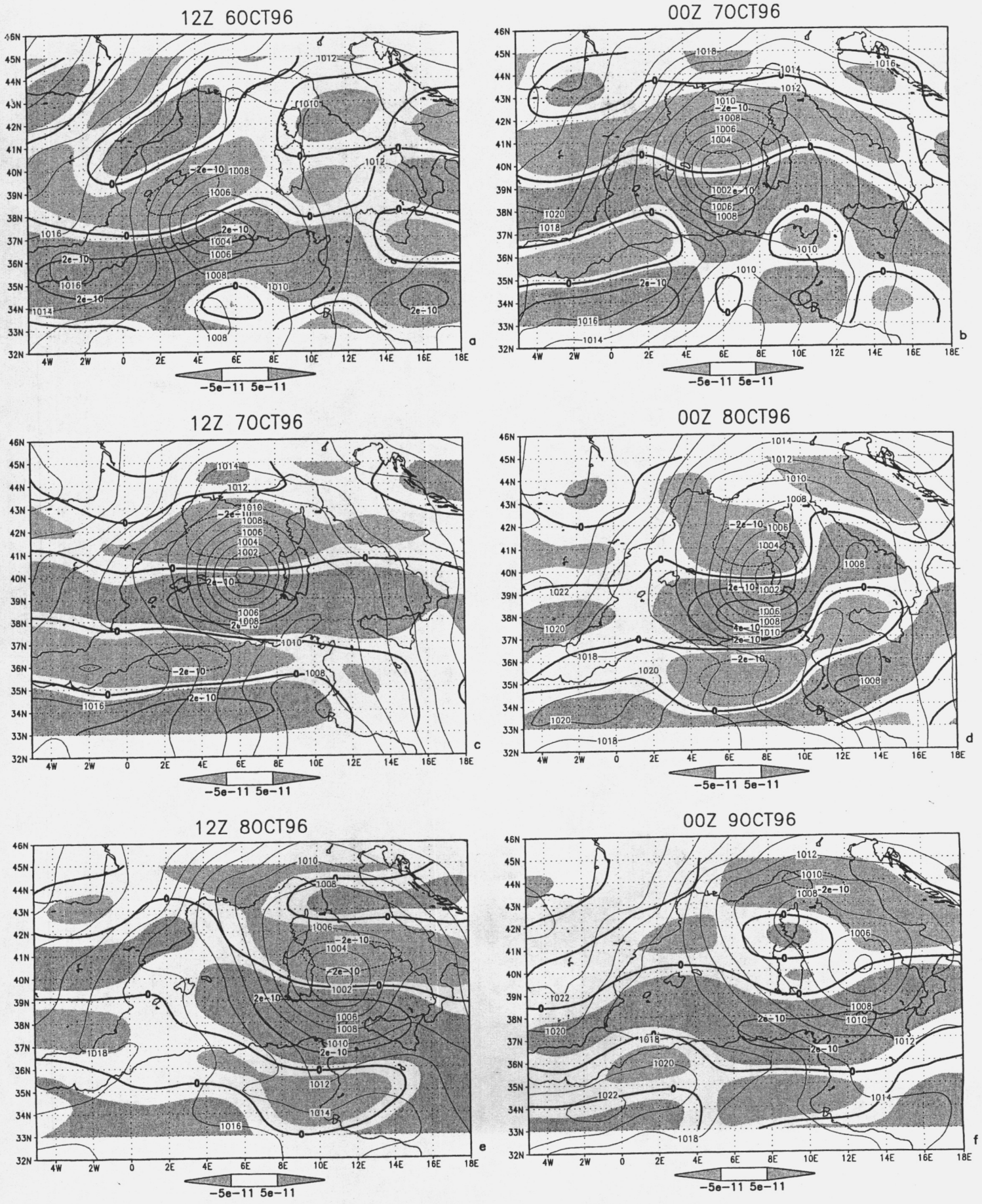
12Z 60CT96
00Z 70CT96
12Z 70CT96
00Z 80CT96
12Z 80CT96
00Z 90CT96
-5e-11 5e-11
a
b
c
d
e
f

Fig 2

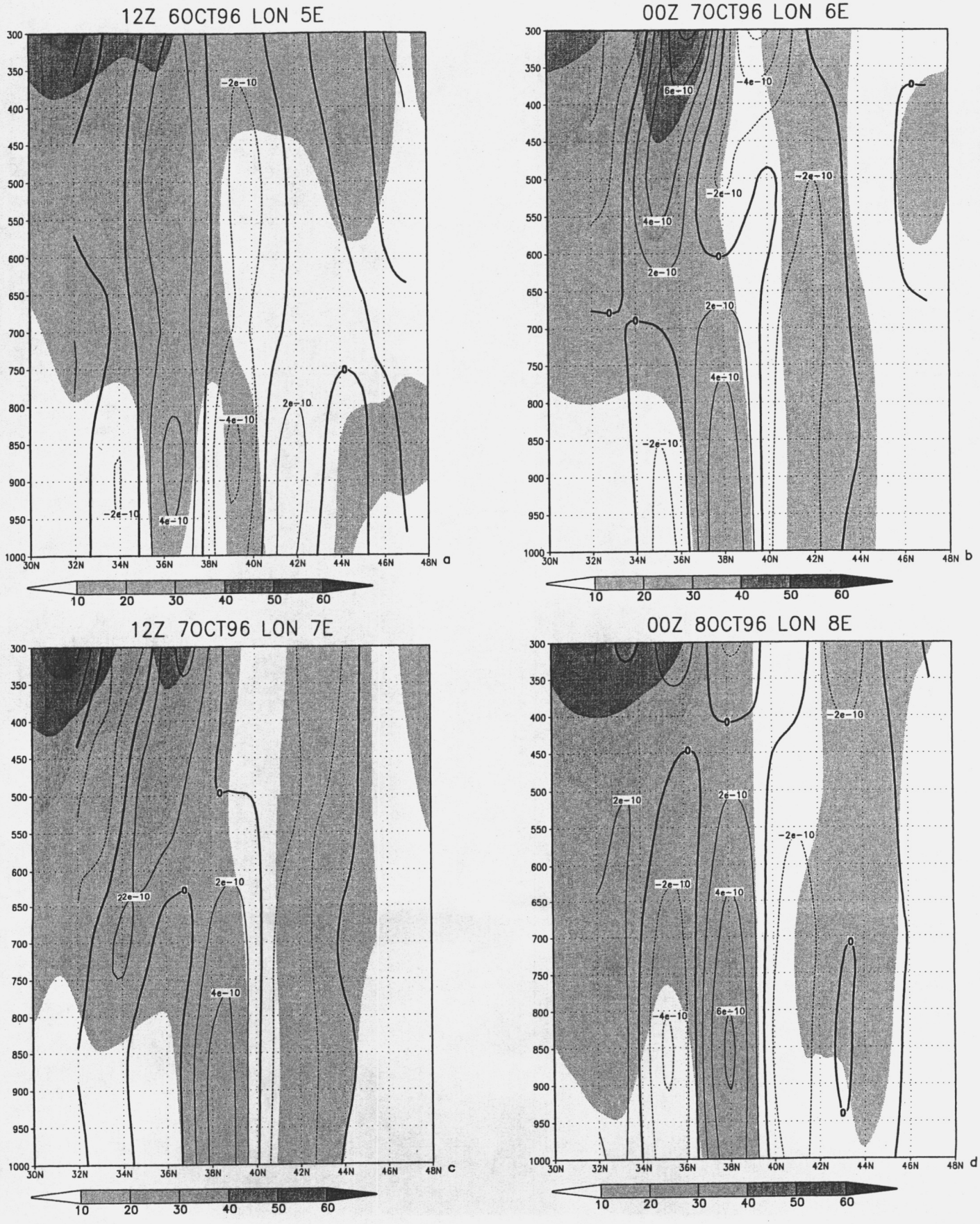
12Z 6OCT96 LON 5E
00Z 7OCT96 LON 6E
12Z 7OCT96 LON 7E
00Z 8OCT96 LON 8E
a
b
c
d
10 20 30 40 50 60
30N 32N 34N 36N 38N 40N 42N 44N 46N 48N

Fig 3

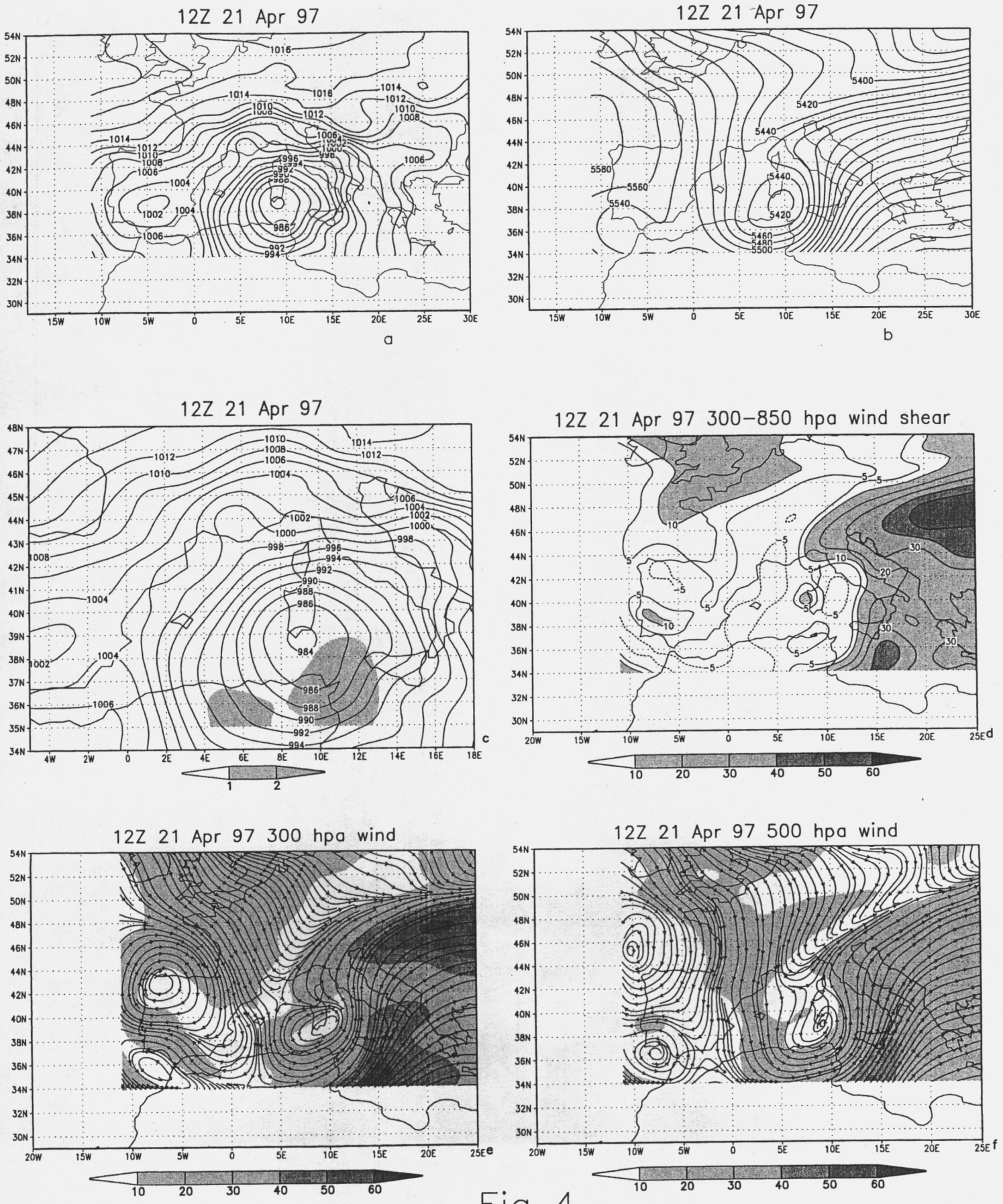
12Z 21 Apr 97
a
12Z 21 Apr 97
b
12Z 21 Apr 97
c
12Z 21 Apr 97 300–850 hpa wind shear
d
12Z 21 Apr 97 300 hpa wind
e
12Z 21 Apr 97 500 hpa wind
f

Fig 4

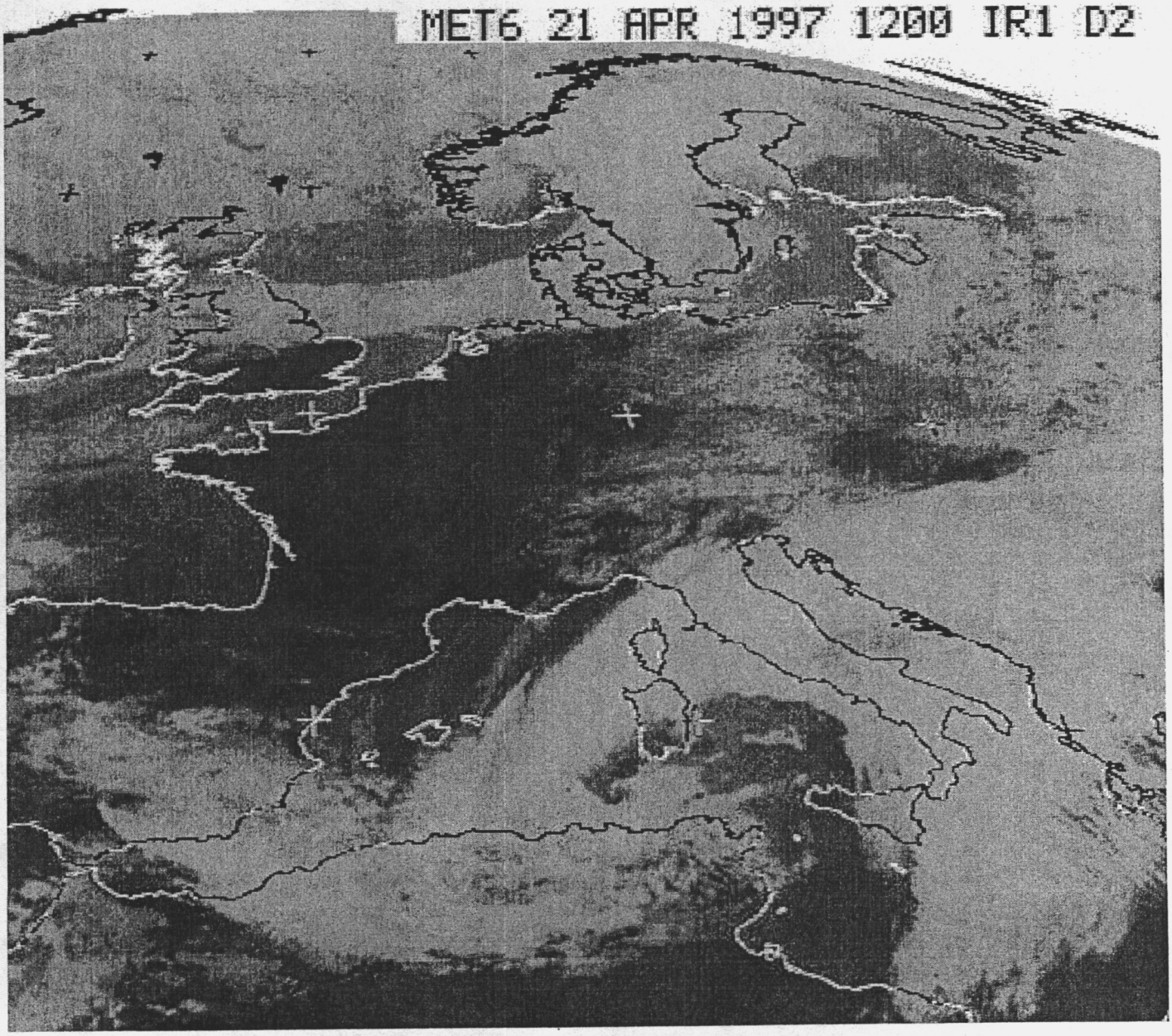

Fig 5

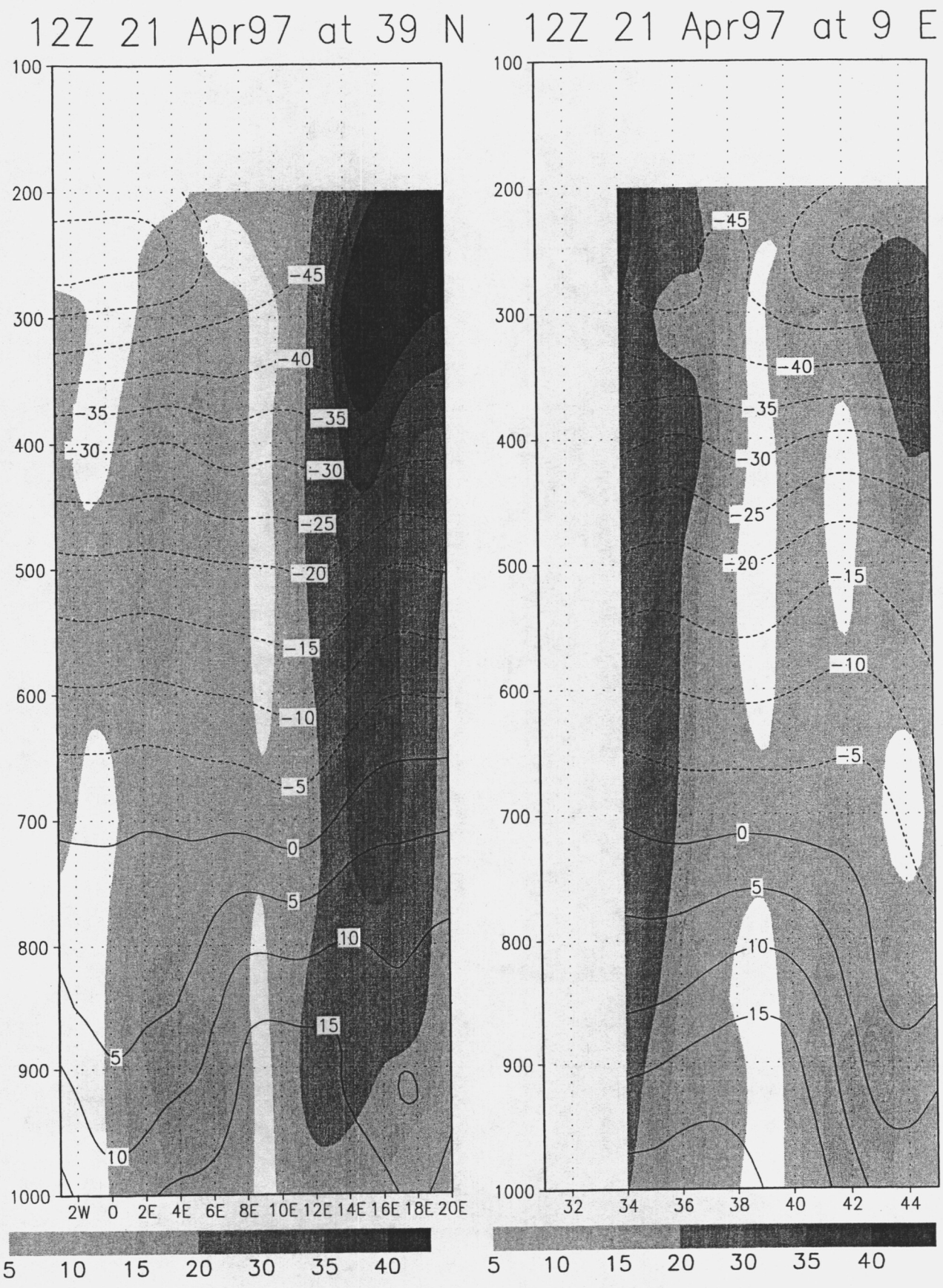
12Z 21 Apr97 at 39 N
12Z 21 Apr97 at 9 E
100
200
300
400
500
600
700
800
900
1000
-45
-40
-35
-30
-25
-20
-15
-10
-5
0
5
10
15
2W 0 2E 4E 6E 8E 10E 12E 14E 16E 18E 20E
32 34 36 38 40 42 44
5 10 15 20 30 35 40

Fig 6

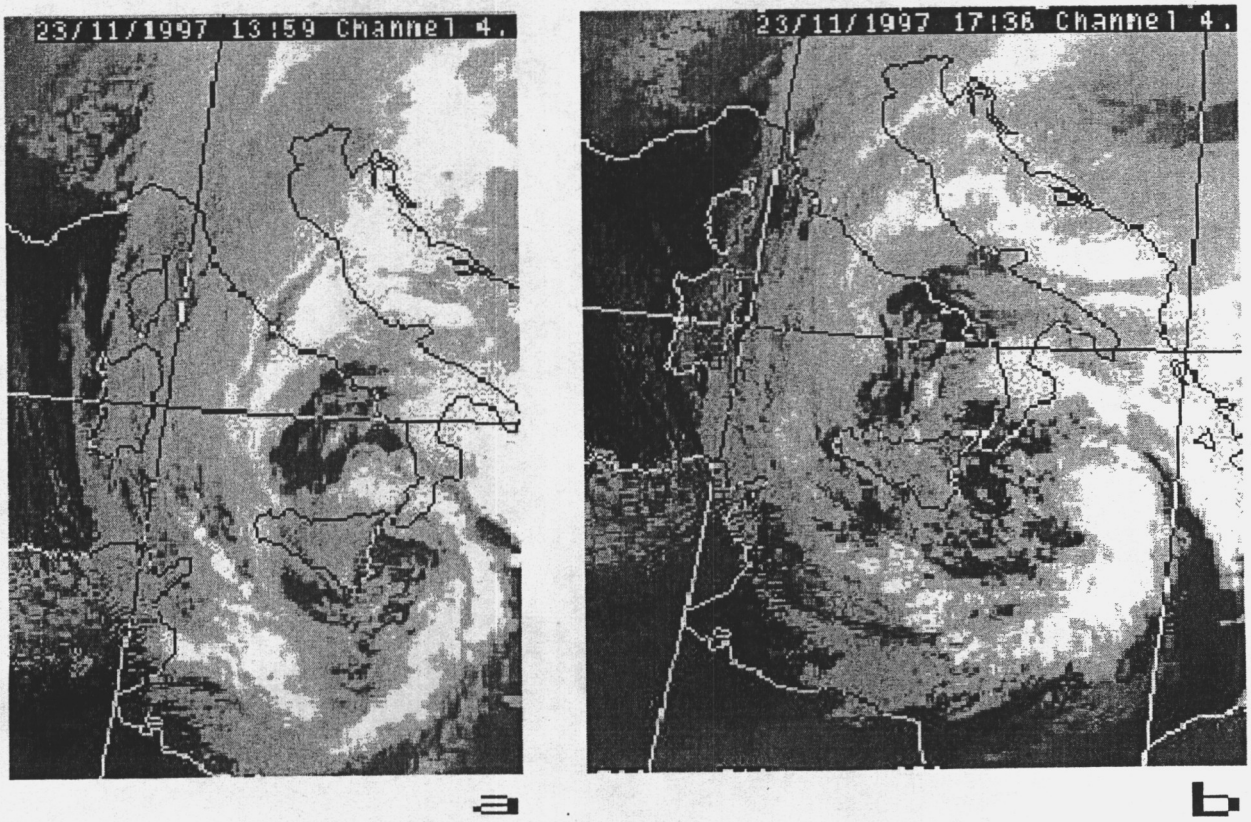

Fig 7

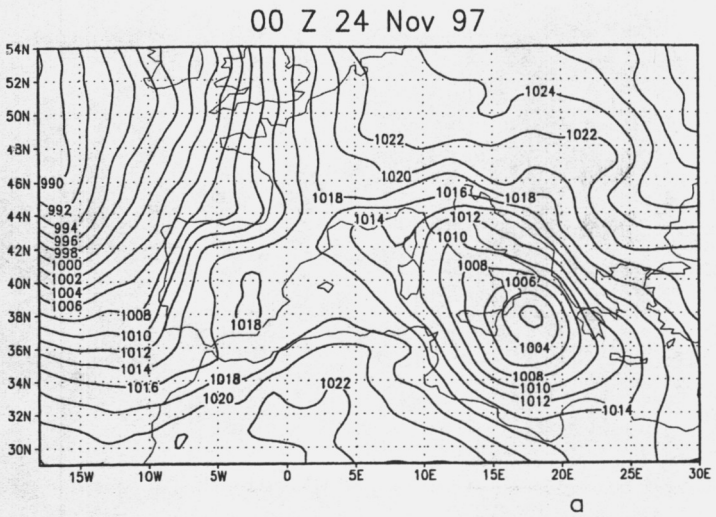
00 Z 24 Nov 97

a

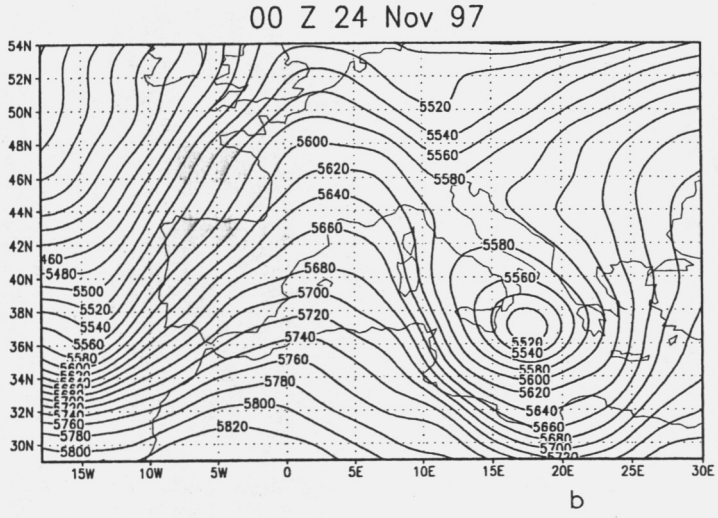
00 Z 24 Nov 97

b

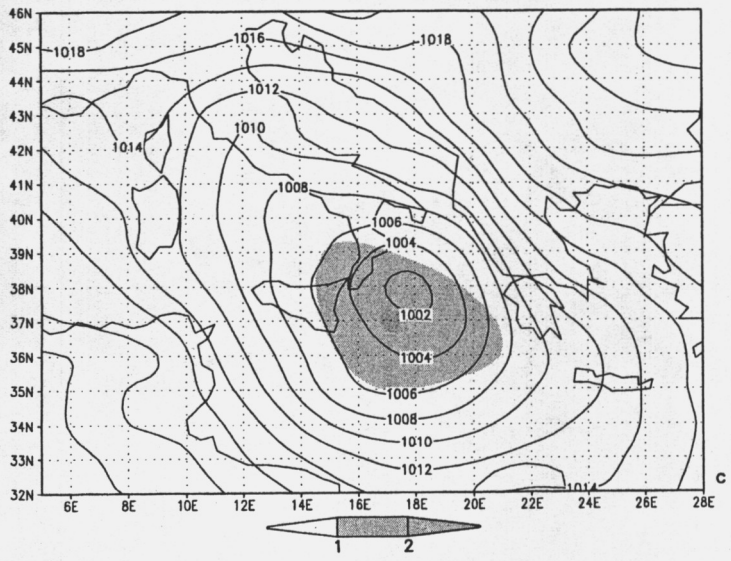
00Z 24 Nov 97

c

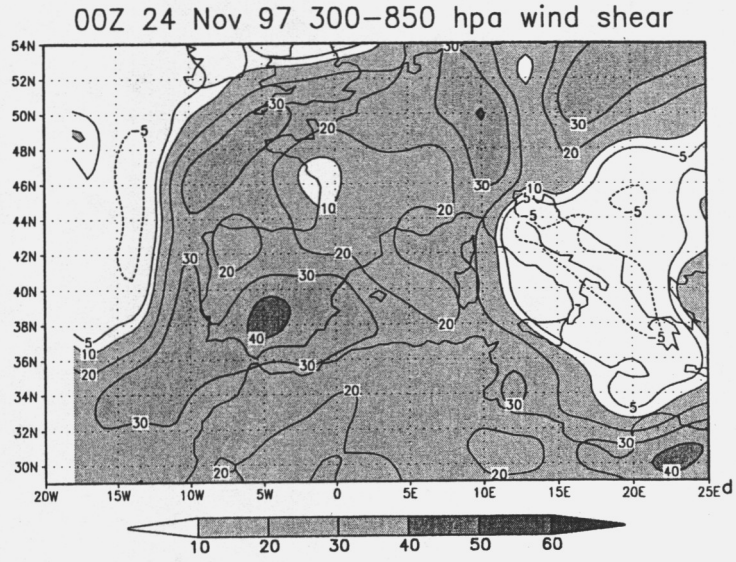
00Z 24 Nov 97 300–850 hpa wind shear

d

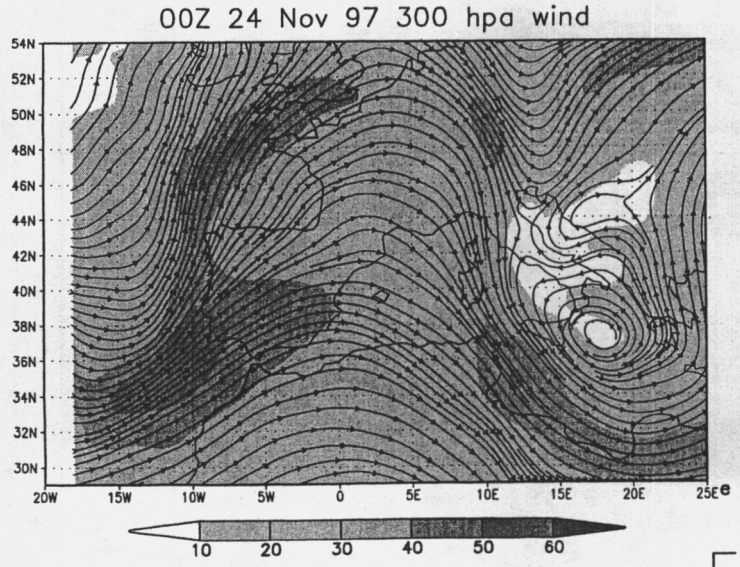
00Z 24 Nov 97 300 hpa wind

e

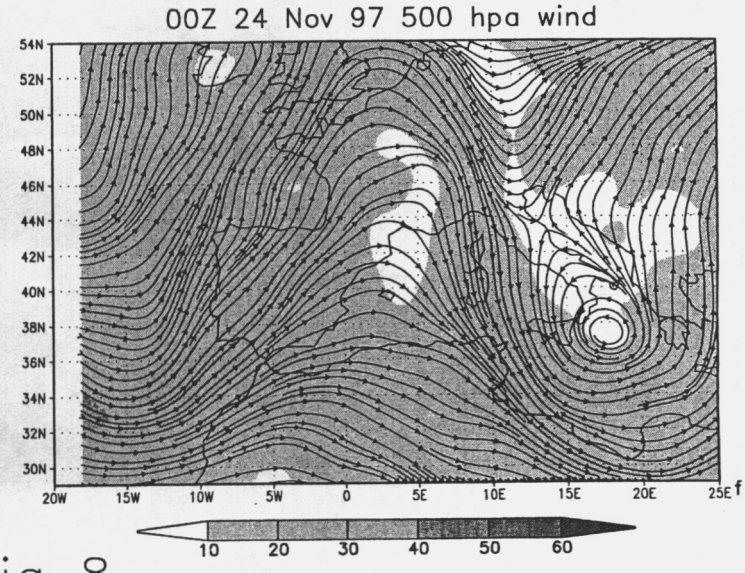
00Z 24 Nov 97 500 hpa wind

f

Fig 8

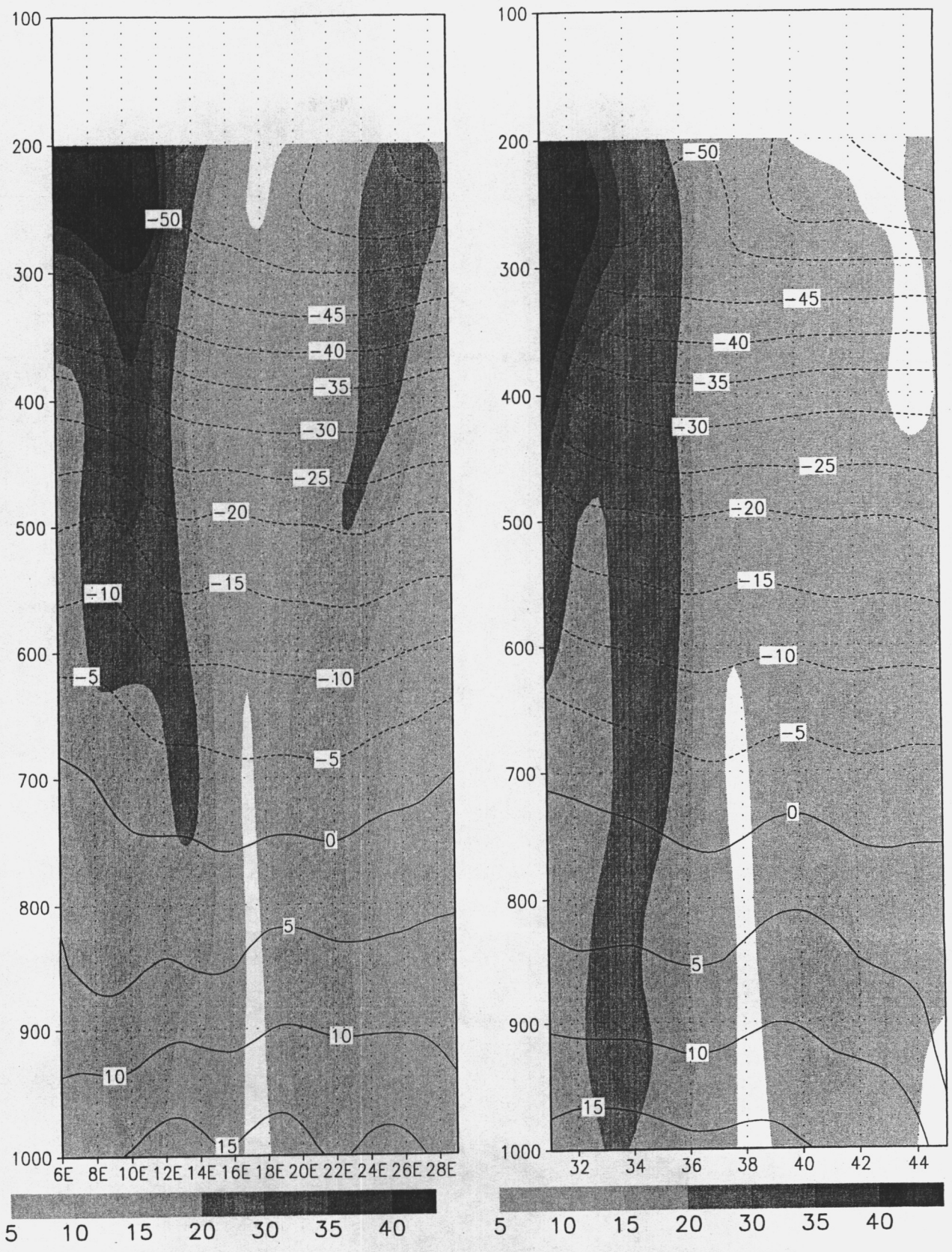
00Z 24 Nov97 at 38 N
00Z 24 Nov97 at 17 E
100
200
300
400
500
600
700
800
900
1000
-50
-45
-40
-35
-30
-25
-20
-15
-10
-5
0
5
10
15
6E 8E 10E 12E 14E 16E 18E 20E 22E 24E 26E 28E
32 34 36 38 40 42 44
5 10 15 20 30 35 40

Fig 9

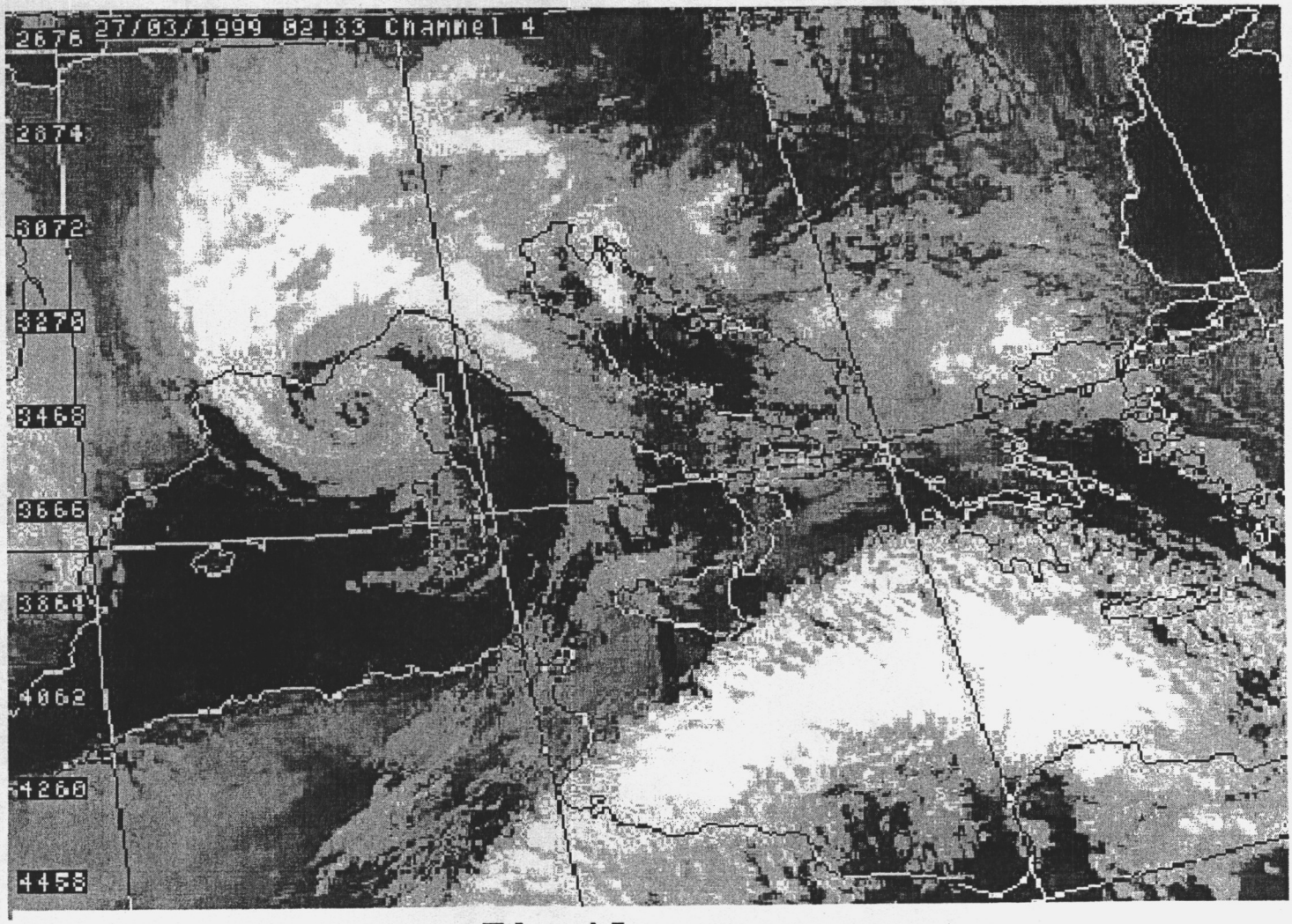
2676 27/03/1999 02:33 Channel 4
2874
3072
3270
3468
3666
3864
4062
4260
4458

Fig 10

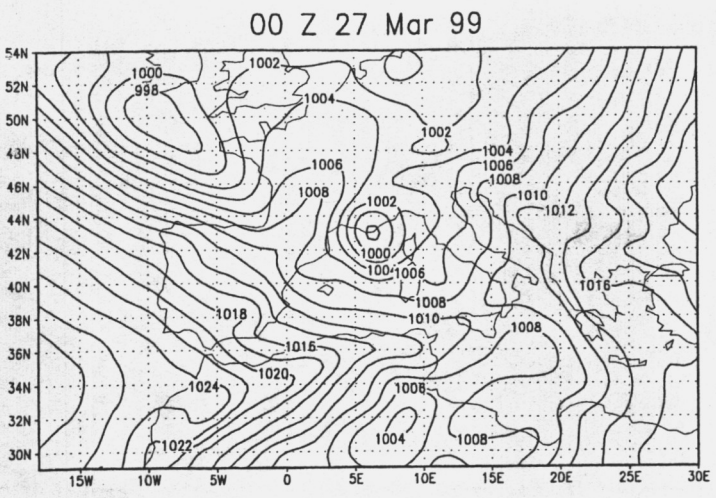
00 Z 27 Mar 99
a

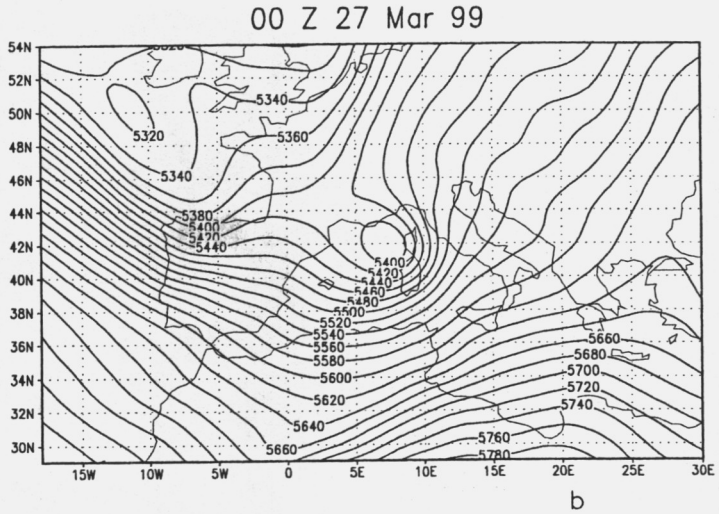
00 Z 27 Mar 99
b

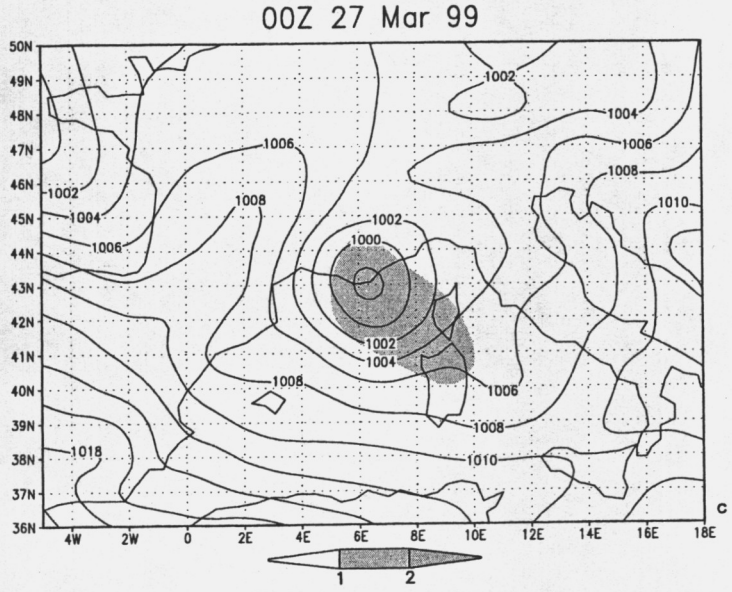
00Z 27 Mar 99
c

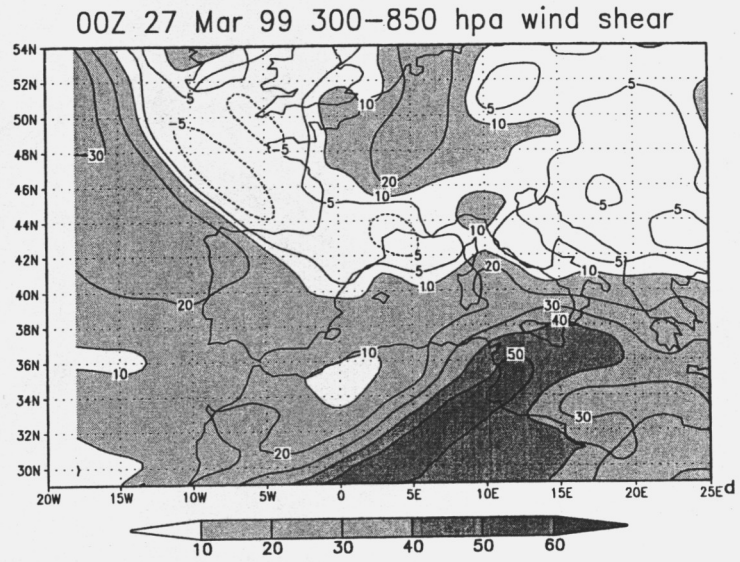
00Z 27 Mar 99 300–850 hpa wind shear
d

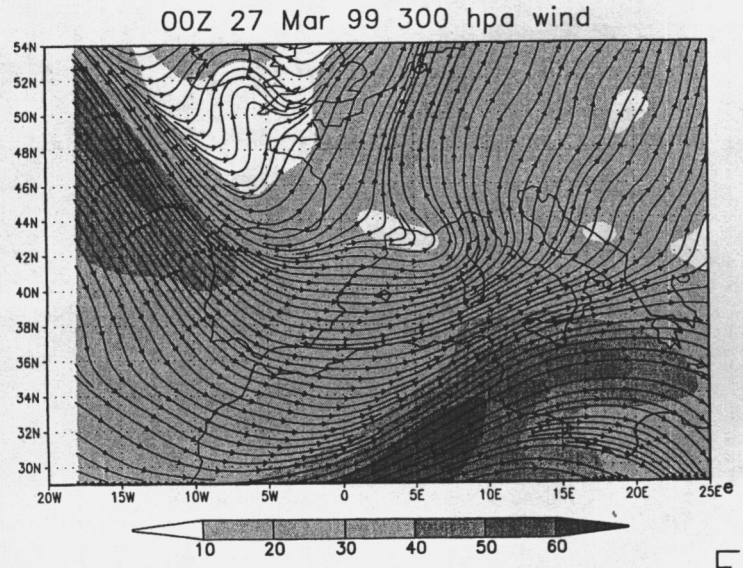
00Z 27 Mar 99 300 hpa wind
e

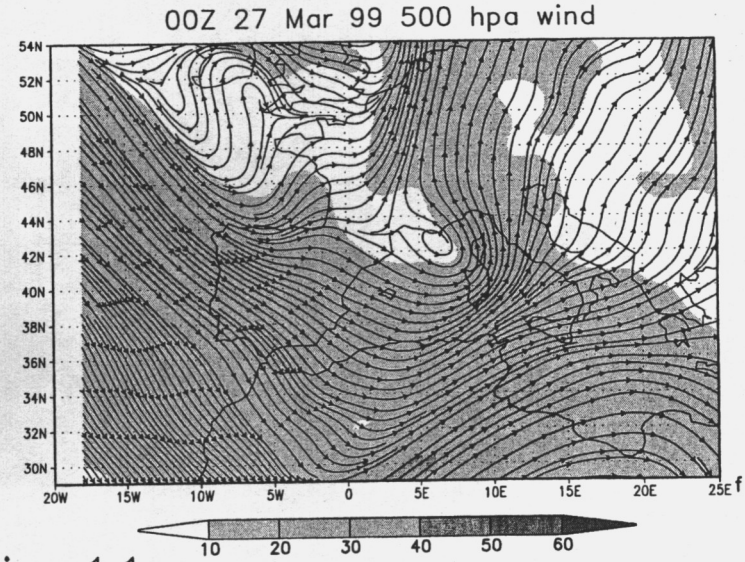
00Z 27 Mar 99 500 hpa wind
f

Fig 11

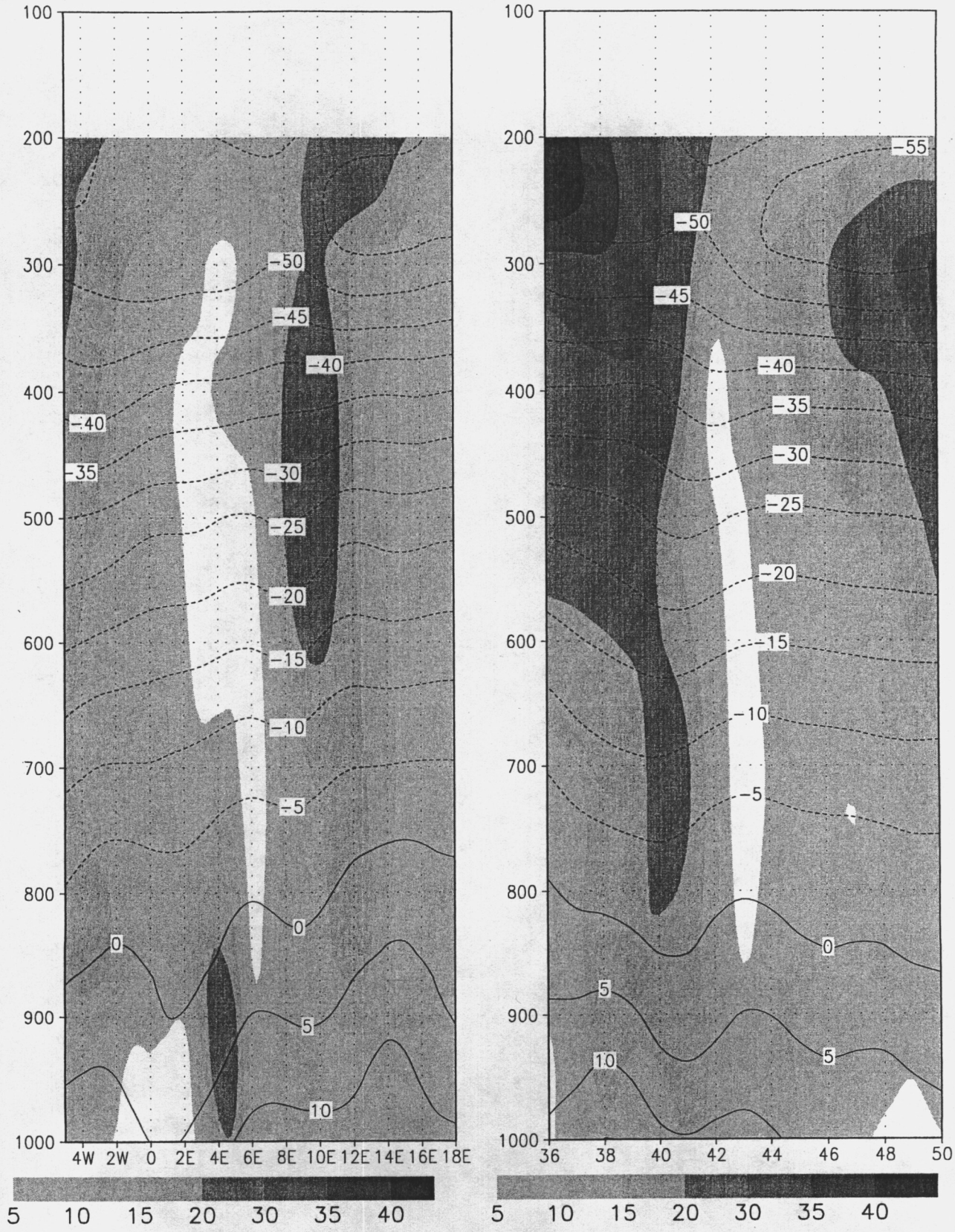
00Z 27 Mar99 at 40 N
00Z 27 Mar99 at 6 E
100
200
300
400
500
600
700
800
900
1000
-50
-45
-40
-35
-30
-25
-20
-15
-10
-5
0
5
10
-55
4W 2W 0 2E 4E 6E 8E 10E 12E 14E 16E 18E
36 38 40 42 44 46 48 50
5 10 15 20 30 35 40
5 10 15 20 30 35 40

Fig 12

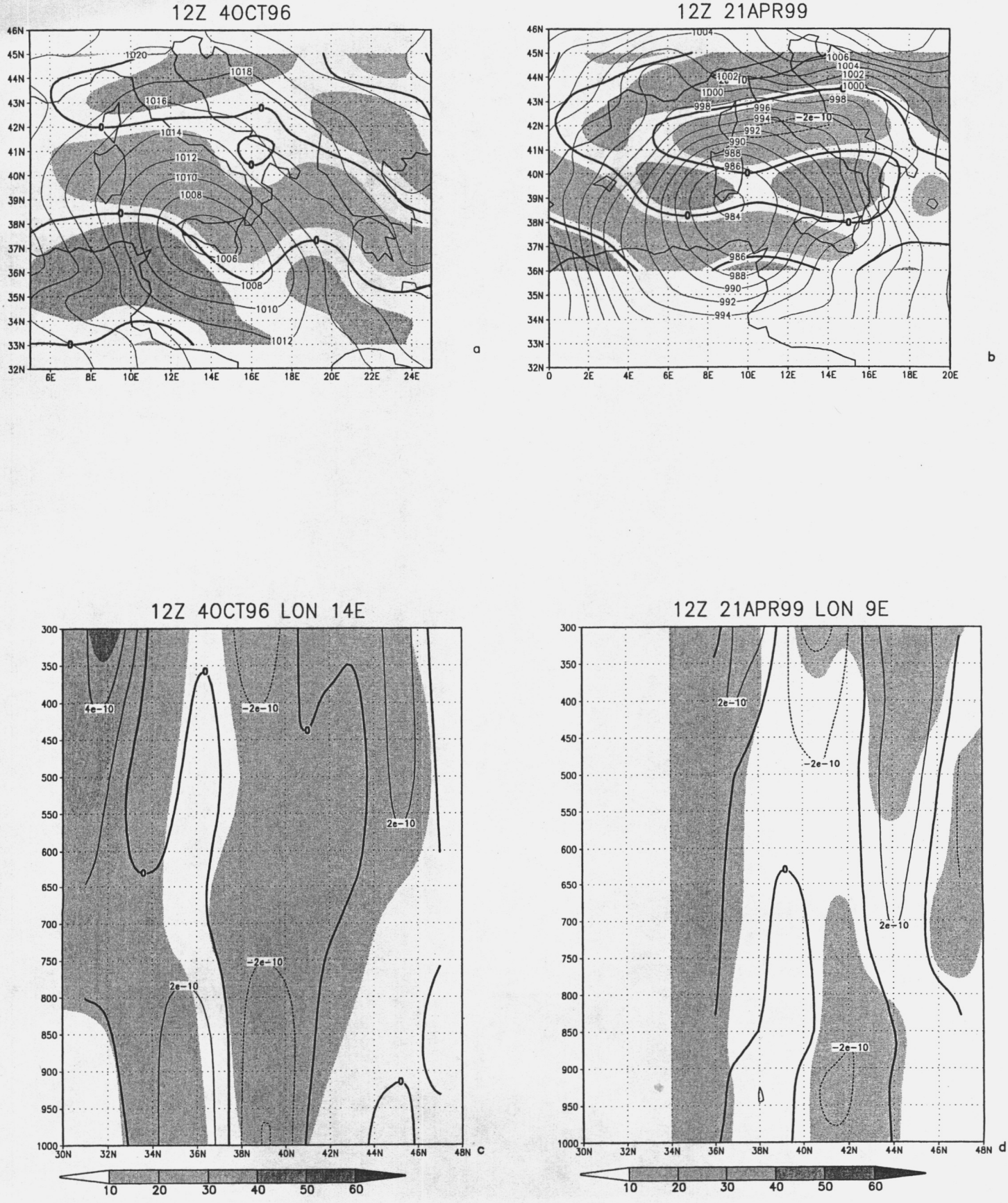
12Z 40CT96
12Z 21APR99
a
b
12Z 40CT96 LON 14E
12Z 21APR99 LON 9E
c
d
4e-10
-2e-10
2e-10
10
20
30
40
50
60

Fig 13

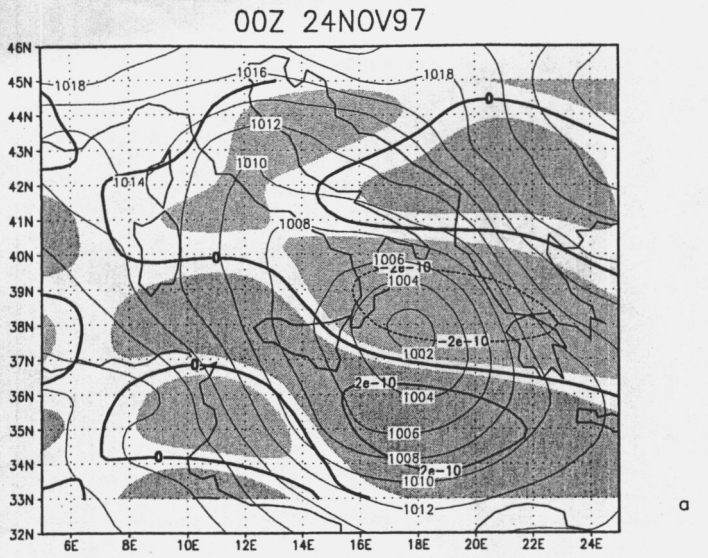
00Z 24NOV97
46N
45N
44N
43N
42N
41N
40N
39N
38N
37N
36N
35N
34N
33N
32N
6E
8E
10E
12E
14E
16E
18E
20E
22E
24E
1018
1016
1012
1010
1014
1008
1006
1004
1002
1000
-2e-10
2e-10
0

a

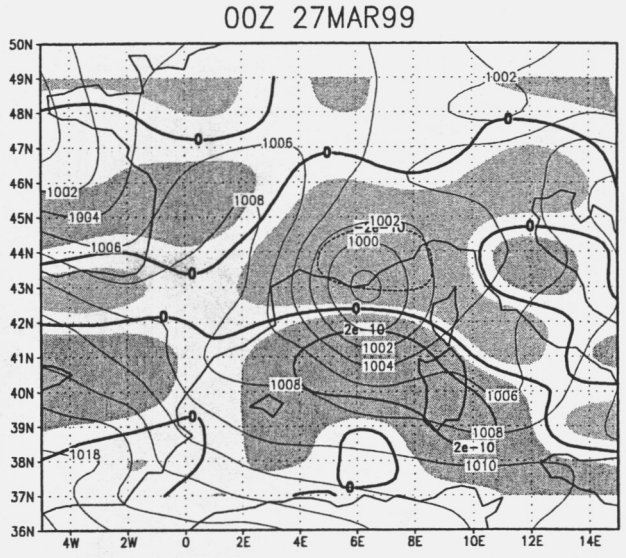
00Z 27MAR99
50N
49N
48N
47N
46N
45N
44N
43N
42N
41N
40N
39N
38N
37N
36N
4W
2W
0
2E
4E
6E
8E
10E
12E
14E
1002
1004
1006
1008
1000
2e-10
1010
1018
0

b

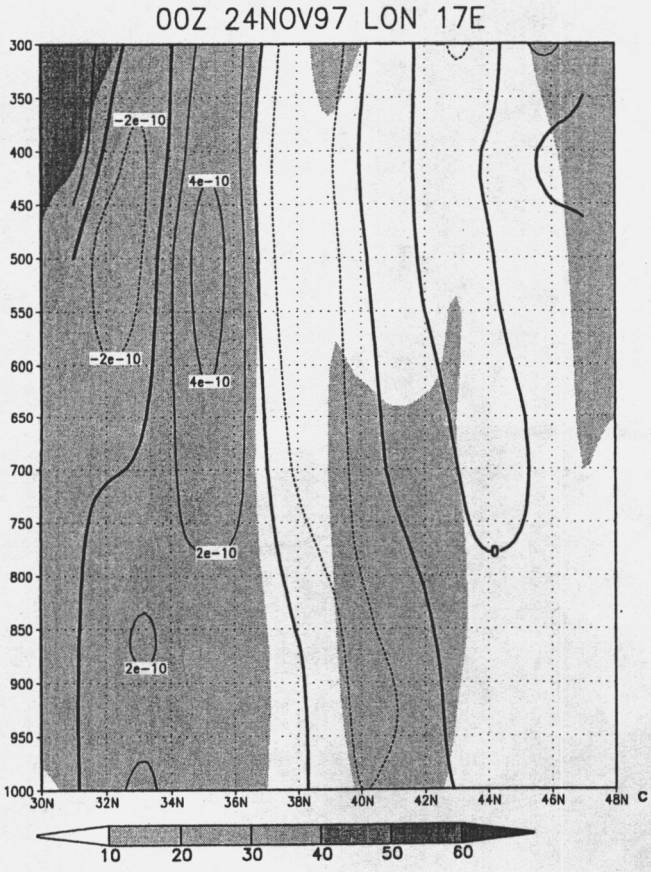
00Z 24NOV97 LON 17E
300
350
400
450
500
550
600
650
700
750
800
850
900
950
1000
30N
32N
34N
36N
38N
40N
42N
44N
46N
48N
-2e-10
4e-10
2e-10
0
10
20
30
40
50
60

c

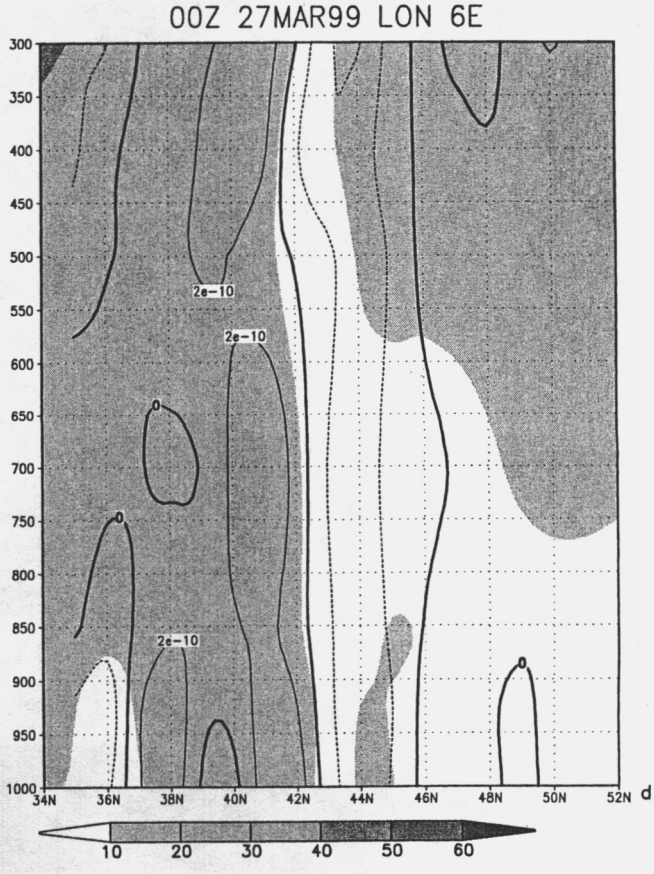
00Z 27MAR99 LON 6E
300
350
400
450
500
550
600
650
700
750
800
850
900
950
1000
34N
36N
38N
40N
42N
44N
46N
48N
50N
52N
2e-10
0
10
20
30
40
50
60

d

Fig 14

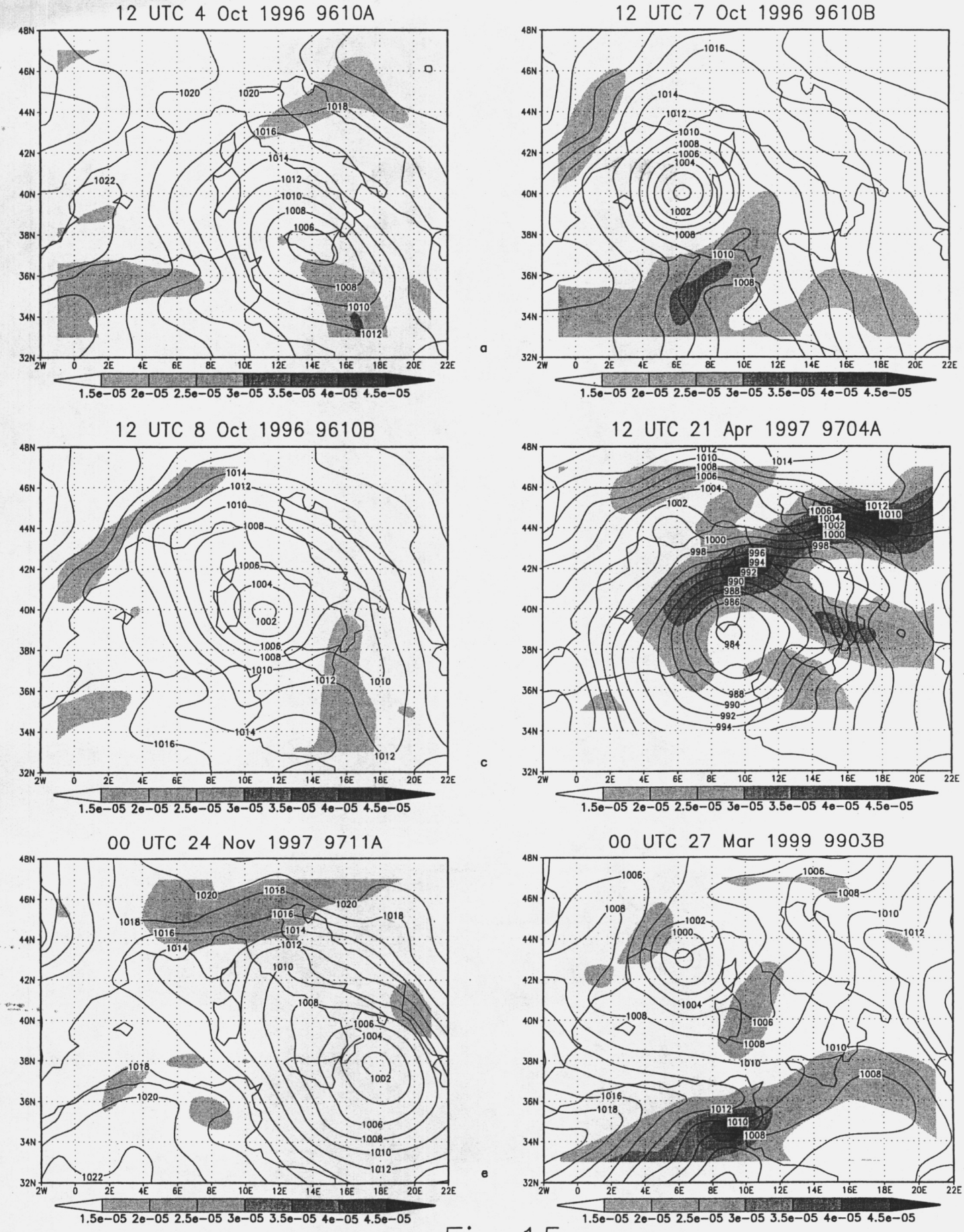
12 UTC 4 Oct 1996 9610A
12 UTC 7 Oct 1996 9610B
12 UTC 8 Oct 1996 9610B
12 UTC 21 Apr 1997 9704A
00 UTC 24 Nov 1997 9711A
00 UTC 27 Mar 1999 9903B
a
b
c
d
e
f
1.5e-05 2e-05 2.5e-05 3e-05 3.5e-05 4e-05 4.5e-05

Fig 15